AN ELECTROMAGNETIC TOOL FOR DAMPING AND FATIGUE ANALYSIS

THESIS

Todd M. Hoover, Captain, USAF

AFIT/GSS/ENY/04-M04

DEPARTMENT OF THE AIR FORCE
AIR UNIVERSITY

AIR FORCE INSTITUTE OF TECHNOLOGY

Wright-Patterson Air Force Base, Ohio

APPROVED FOR PUBLIC RELEASE; DISTRIBUTION UNLIMITED

The views expressed in this thesis are those of the author and do not reflect the official policy or position of the United States Air Force, Department of Defense, or the United States Government.

AFIT/GSS/ENY/04-M04

AN ELECTROMAGNETIC TOOL FOR DAMPING AND FATIGUE ANALYSIS

THESIS

Presented to the Faculty

Department of Aeronautics and Astronautics

Graduate School of Engineering and Management

Air Force Institute of Technology

Air University

Air Education and Training Command

In Partial Fulfillment of the Requirements for the

Degree of Master of Science (Space Systems)

Todd M. Hoover, BS

Captain, USAF

March 2004

APPROVED FOR PUBLIC RELEASE; DISTRIBUTION UNLIMITED.

AFIT/GSS/ENY/04-M04

AN ELECTROMAGNETIC TOOL FOR DAMPING AND FATIGUE ANALYSIS

Todd M. Hoover, BS
Captain, USAF

Approved:

/signed/	
Anthony N. Palazotto (Chairman)	date
/signed/	
Richard G. Cobb (Member)	date
/signed/	
William D. Wood (Member)	date

Abstract

An automated test system was developed by the USAF Turbine Engine Fatigue Facility (TEFF). This system was initially designed to reduce the time and manpower required to characterize damping treatments. It is based on a digitally controlled environmental chamber with automated data acquisition and processing. Several outputs are available including identification of natural frequencies, modal damping ratios from the acquired frequency responses, and changes in damping with response amplitude [7]; however, the TEFF additionally desires the capability to study fatigue under a free boundary condition.

The system consists of a test specimen suspended by a pendulum to closely simulate free boundary conditions and to minimize the dissipation of vibrational energy. Two rare earth magnets are attached to a specimen. The magnetized end is inserted into an orthogonal magnetic field produced by an electromagnet. Alternating the current oscillates the direction of the magnetic field by 180 degrees. The effect of the electromagnet's magnetic field on the specimen's magnets is the application of a torque; as this torque alternates directions, it excites vibration in the beam. This torque, while useful, was not fully understood. The purpose of this thesis is threefold: 1. Develop an equation to predict the magnetic field produced by an electromagnetic coil;
2. Develop an equation for predicting the torque exerted on the beam; and
3. Experimentally validate the accuracy of these equations.

Acknowledgments

I would like to thank my thesis advisor, Dr. Anthony Palazotto, for his time, support, and effort with this thesis. His guidance and friendship made this research much better than I could have done on my own. Additionally, I would like to express my appreciation to my sponsor, Dr. Charles Cross, from the Air Force Research Lab's Turbine Engine Fatigue Facility (TEFF), for giving a non-mechanical engineering guy the opportunity to do a mechanical engineering thesis.

I am, also, indebted to the many professionals at the TEFF who spent time with me, especially Tommy George, Brian Runyon, and Gary Terborg. Regardless of what else was happening at the time, you always took time out of your schedule to assist and advise me.

I would also like to thank Majors William Wood and Clark Groves of the AFIT faculty. I thought I understood electromagnetism until I talked to you.

Finally, where would I be without my family! You put as much time into AFIT as I did. Your love and support makes it all worth while.

Todd M. Hoover

Table of Contents

Page

List of Figures

Figure Page

Figure Page

List of Tables

List of Units

Abbreviation	Unit	Explanation	Equals
A	ampere/amp	rate of flow of charge	C/s
C	coulomb	electric charge	fundamental unit
ft	foot	length	fundamental unit
G	gauss	magnetic field/magnetic flux density	10^{-4} T
g	gram	mass	fundamental unit
H	henry	inductance	V-s/A
h	hour	time	fundamental unit
Hz	hertz	number of cycles per second	cycles/s
in	inch	length	fundamental unit
J	joules	energy	kg-m^2/s^2
lb	pound	force	slug-ft/s^2
m	meter	length	fundamental unit
min	minute	time	fundamental unit
N	newton	force	kg-m/s^2
s	second	time	fundamental unit
slug	slug	mass	fundamental unit
T	tesla	magnetic field or magnetic flux density	N/A-m
V	volt	energy per unit charge	J/s
Wb	weber	magnetic flux	T-m^2

List of Symbols

Symbol	Unit	Explanation
A	m^2	area
$\vec{A}$	m^2	area vector of a current loop (see Appendix A)
$\vec{B}$	T	magnetic field vector (see Appendix A)
$\vec{B}_i$	T	intrinsic magnetic field vector of a magnet (see Appendix A)
B_x, B_y	T	components of $\vec{B}$ in the x and y directions
$\vec{d}$	m	length vector of moment arm
$d\vec{A}$	m^2	differential area vector of a current loop (see Appendix A)
$d\vec{B}$	T	differential magnetic field vector
dB_x, dB_y	T	differential components of $\vec{B}$ in the x and y directions
dI	A	differential current
dR	m	differential radial length
$d\vec{s}$	m	differential length in the direction of current flow
dx	m	differential longitudinal length
$d\vec{F}$	N	differential force vector
$d\vec{m}$	$A\text{-}m^2$	differential magnetic dipole moment vector (see Appendix A)
dV	m^3	differential volume
$\vec{F}$	N	force vector
I	A	current
J	A/m^2	current density; current per unit area

K ..... none ..... magnetic dipole moment scaling factor (a constant)

k ..... none ..... relative permeability (see Appendix A)

k_m ..... Wb/A-m .. a constant equal to $m_o/4p$

l ..... m ..... length

$\vec{M}$ ..... A/m ..... magnetization vector (see Appendix A)

$\vec{m}$ ..... A- m^2 ..... magnetic dipole moment vector (see Appendix A)

N ..... none ..... number of turns of wire on a coil

n ..... turns/m .... number of turns of wire on a coil per unit length

p ..... none 3.141592654

R ..... m ..... radial length

R_1, R_2 ..... m ..... respectively, inner and outer radius of a coil

r ..... m ..... distance

$\vec{t}$ ..... N-m ..... torque vector

$\vec{t}_e$ ..... N-m ..... experimentally measured torque vector

q ..... degrees .... angular measurement

m ..... Wb/A-m .. magnetic permeability of a material (see Appendix A)

m_o ..... Wb/A-m .. permeability of free space (see Appendix A)

V ..... m^3 ..... volume

x ..... m ..... distance

x_1 ..... m ..... distance; near side of coil to magnetic field measurement point

x_2 ..... m ..... distance; far side of coil to magnetic field measurement point

List of Notations

Notation Explanation

A .....scalar quantity or magnitude of a vector

$\vec{B}$ .....denotes a vector

$\hat{r}$ .....denotes a unit vector in the direction of r

∇ .....del operator

$A \cdot \vec{B}$ .....multiplication

$\vec{A} \bullet \vec{B}$ .....scalar product or dot product of vectors

$\vec{A} \times \vec{B}$ .....cross product or vector product of vectors

AN ELECTROMAGNETIC TOOL FOR DAMPING AND FATIGUE ANALYSIS

I. Introduction

Fatigue

When designing structures, engineers seek to incorporate a design which is capable of handling some critical level of stress. The material(s) being used in the design dictates the amount of stress the structure will be able withstand. However, when dealing with cyclic loading, structures can fail at stress values much lower than the ultimate stress of the material [1]. This cyclic loading can be divided into two categories: Low Cycle Fatigue (LCF) and High Cycle Fatigue (HCF). The two key differences between LCF and HCF are load levels and the resultant fatigue life.

LCF loads are higher resulting in fatigue lives less than 10,000 cycles. HCF loads are lower and, as such, in the elastic range; therefore, fatigue lives exceed 10,000 cycles [2]. HCF failures can occur quickly due to high frequency loading [3].

High Cycle Fatigue in Aircraft Engines

Since the dawn of the jet age, one of the major limiting factors to the lifespan of jet engines is fatigue in turbo machinery blades. Blade fatigue is brought on by both Low and High Cycle Fatigue. Fortunately, through the use of fracture mechanics and a retirement-for-cause management philosophy, LCF failures in aircraft engines have been greatly reduced [1]. As a result, HCF is the primary cause of engine failures [4].

Preventing failure of turbo machinery blades "is one of the major objectives of current Air Force HCF programs" [5]. In order to proactively address HCF failure, the National High Cycle Fatigue Initiative was started in 1995 [6]. In 1998, the Air Force Research Laboratory's Propulsion Directorate (AFRL/PR) felt it would be advantageous to develop their own research capability; as such, the Turbine Engine Fatigue Facility (TEFF) was created to investigate HCF [6]. Throughout their tenure, among other things, the TEFF has sought to characterize HCF and explore various damping techniques to eliminate or reduce its impacts. To that end, "an automated test system was developed to reduce the time and manpower required to characterize the effectiveness of damping treatments" [7].

Investigation of Damping and Fatigue

Material damping characterization, and ultimately fatigue analysis, is challenging because the effectiveness of the material in dissipating energy is often temperature, frequency, and strain dependent [8,9]. According to Jones, et al, "Investigating any single material results in a large matrix of test conditions, resulting in a time consuming, labor intensive study" [7]. The investigation of damping and fatigue is typically conducted under a fixed-free setup as in a shaker table. While this type of setup is widely used and understood, the characterization of the fixed boundary condition can be extremely difficult [10].

The natural frequency, damping, and fatigue of a specimen is greatly influenced by its boundary conditions. "In a cantilever experiment, slight variations in clamping pressure or alignment can shift the natural frequency, distort the mode shape, and damp

the specimen by dissipating energy through the clamp-beam friction interface. Additionally, with increased temperature, the relative growth of the specimen and test fixture may change the effective loading force as the test progresses from set point to set point" [7]. Furthermore, when examining fatigue, failure typically occurs within the clamp beam-friction interface [10], see Figure 1.

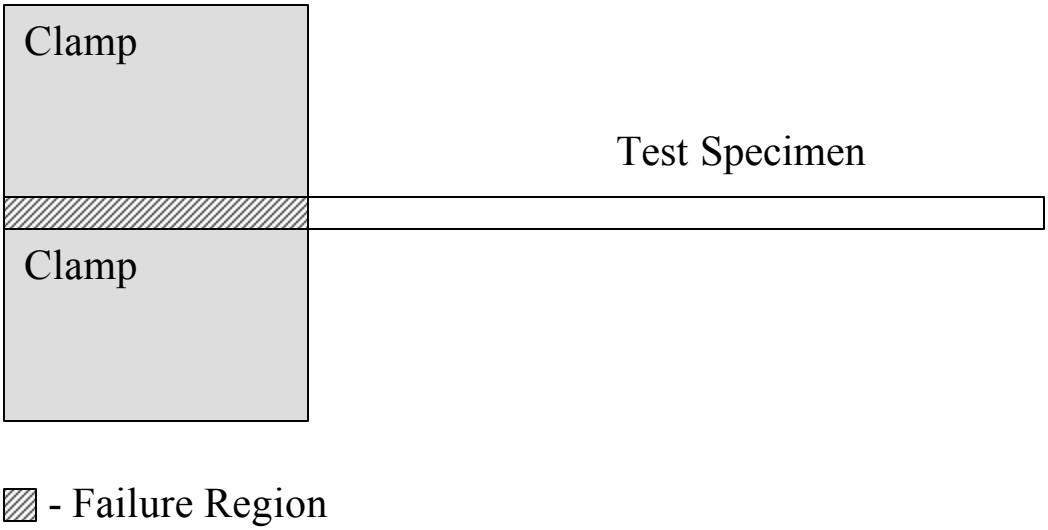

Figure 1. Typical Failure Region in a Cantilever Experiment

In order to reduce, or even eliminate, the need to characterize the boundary conditions at the fixed end and to obtain a more accurate representation of failure, a free-free boundary condition is highly desired. As stated above, the TEFF has developed such a system in order "to greatly reduce the time and manpower required to characterize the effectiveness of various damping treatments such as viscoelastic constrained layer damping and hard coating damping" [7].

Other Free-Free Boundary Condition Setups

While the TEFF has found a viable system for testing turbo machinery blades, their setup is not the only attempt to achieve free boundary conditions. Other organizations, including the Langley Research Center in Hampton, VA [11], among others, are highly interested in valid free-free boundary condition systems for applications outside aircraft engines.

With the ever-increasing demand for assets located in space, free-free boundary condition systems are becoming highly desirable to simulate a zero gravity atmosphere. Structures in space have long dealt with various devices to mitigate vibrational damping in an air-free atmosphere. Unlike air-breathing vehicles, significant vibrations can be introduced into space structures with 1 ms propulsion thrusts, spacecraft docking activities, and movement of equipment such as antennas and cameras. Ongoing research into vibrational damping of space structures makes an affordable, low power system, like that developed by the TEFF, necessary to accurately determine material damping characteristics in their zero gravity or low gravity operating environment.

The TEFF Free-Free Boundary Condition Setup

The TEFF's setup is described by Jones, et al, as follows:

> The mechanical system consists of a digitally controlled environmental chamber, a single point laser vibrometer to measure response and an air-core solenoid to provide electromagnetic excitation to the specimen. Electronically, a function generator is utilized to drive the solenoid and a National Instruments^{TM} input-output card is used to acquire the data and to interface with the environmental chamber and the function generator. All functions are integrated through the use of a LabVIEW^{TM} program to automate and control the test process. Data analysis is conducted through a combination of in-house LabVIEW^{TM} and MATLAB^{TM}

programs as well as the commercially available STAR Modal software. [7]

While this adequately describes the parts of the system, it does not provide enough detail regarding the physical setup of the apparatus which allowed the TEFF to closely simulate free boundary conditions.

A specimen is suspended by a pendulum over a solenoid, see Figure 2. As mentioned above, this suspension closely simulates free boundary conditions while minimizing the dissipation of vibrational energy necessary to obtain a high quality measurement of material damping. The rare earth magnets attached to the specimen account for 18% of the total mass of the specimen. With this mass percentage, Jones, et al, showed there was no significant departure from expected free-free mode shapes [7].

Using ANSYS^{TM} finite element analysis, Jones was able to show the effect the lumped mass has on the mode shapes and natural frequencies of the beam. As indicated in Figure 3 and as stated earlier, the mode shapes resemble free-free beam mode shapes with a shift in the node lines towards the lumped mass. Furthermore, Jones compared the experimentally measured beam natural frequencies to the finite element prediction and the continuous uniform beam theory prediction (see Figure 4) and concluded the lumped mass has a relatively small effect on the beam modes; therefore, the proper normalized strain displacement relationship can be found easily from the finite element analysis [7].

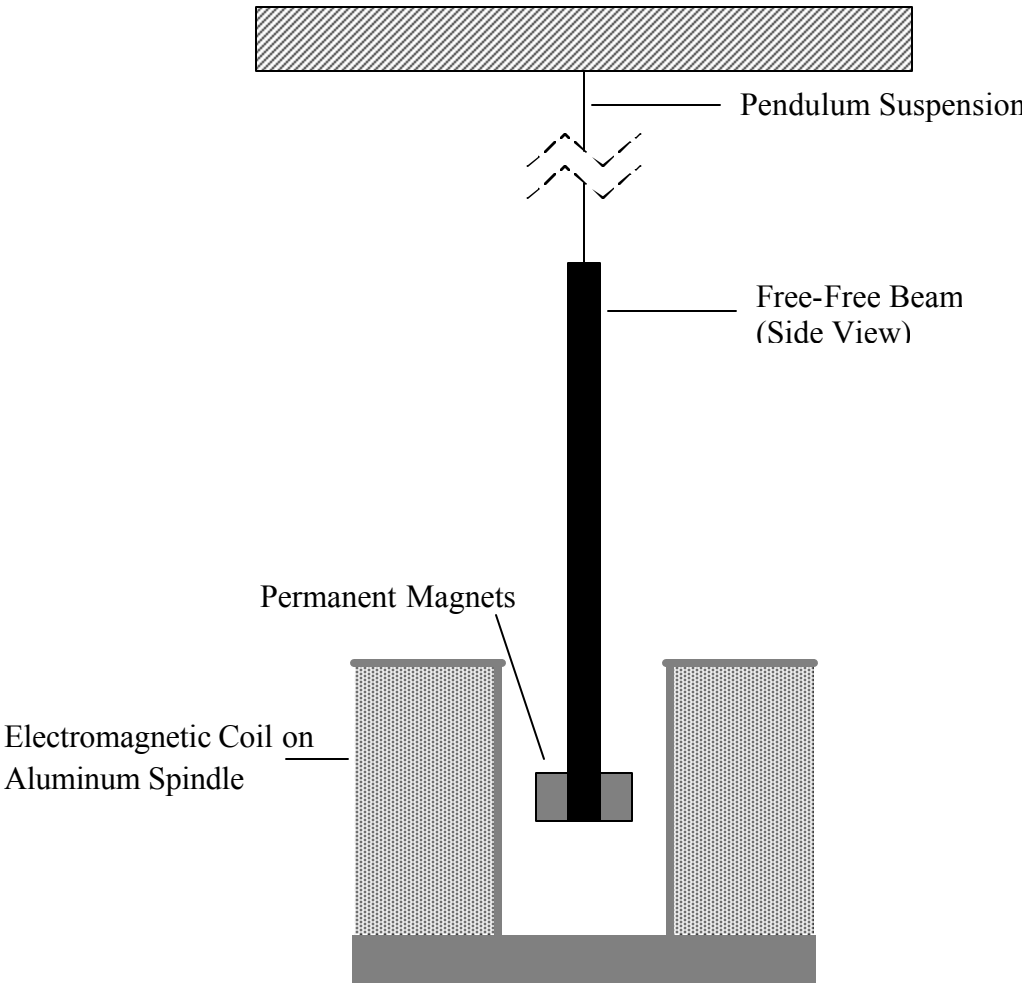

Figure 2. The TEFF "Free-Free" Boundary Condition Setup

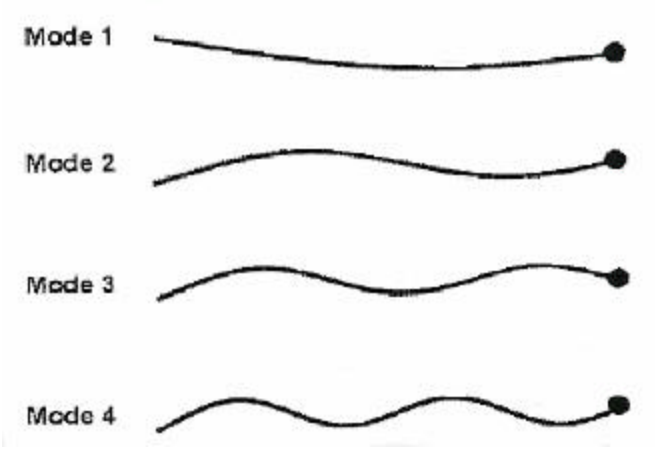

Figure 3. ANSYS ™ Predicted Mode Shapes for Beam with Lumped Mass [7]

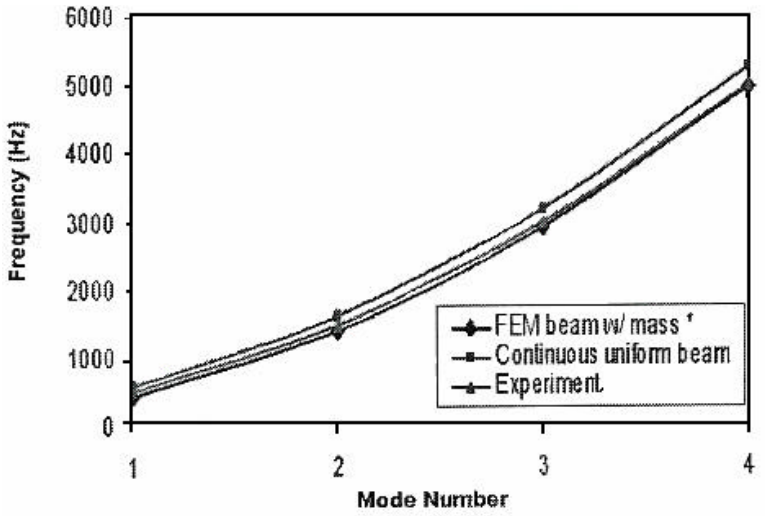

Figure 4. **Comparison of Analytical and Experimental Results for Bare Beam [7]**

While the system is quite simple in its design and configuration, it is quite complex when attempting to model and predict the electromagnetic phenomenon which produces the vibratory excitation of the beam [12, 13].

Magnetic Excitation of Beams

Understanding how the system is setup is essential to discovering how magnets can be used to excite vibration in the beam. The excitation comes from the interaction of two perpendicular magnetic fields: the external field, created by the solenoid, and the magnetic field of the permanent magnets attached to the end of the beam (see Figure 5). When current is applied to the coil, a magnetic field is established running longitudinally through the center of the coil. The permanent magnets experience an applied moment due to this field. Like a compass, the magnetic field lines of the permanent magnet try to line up with the magnetic field lines of the coil. When the current reverses direction, the

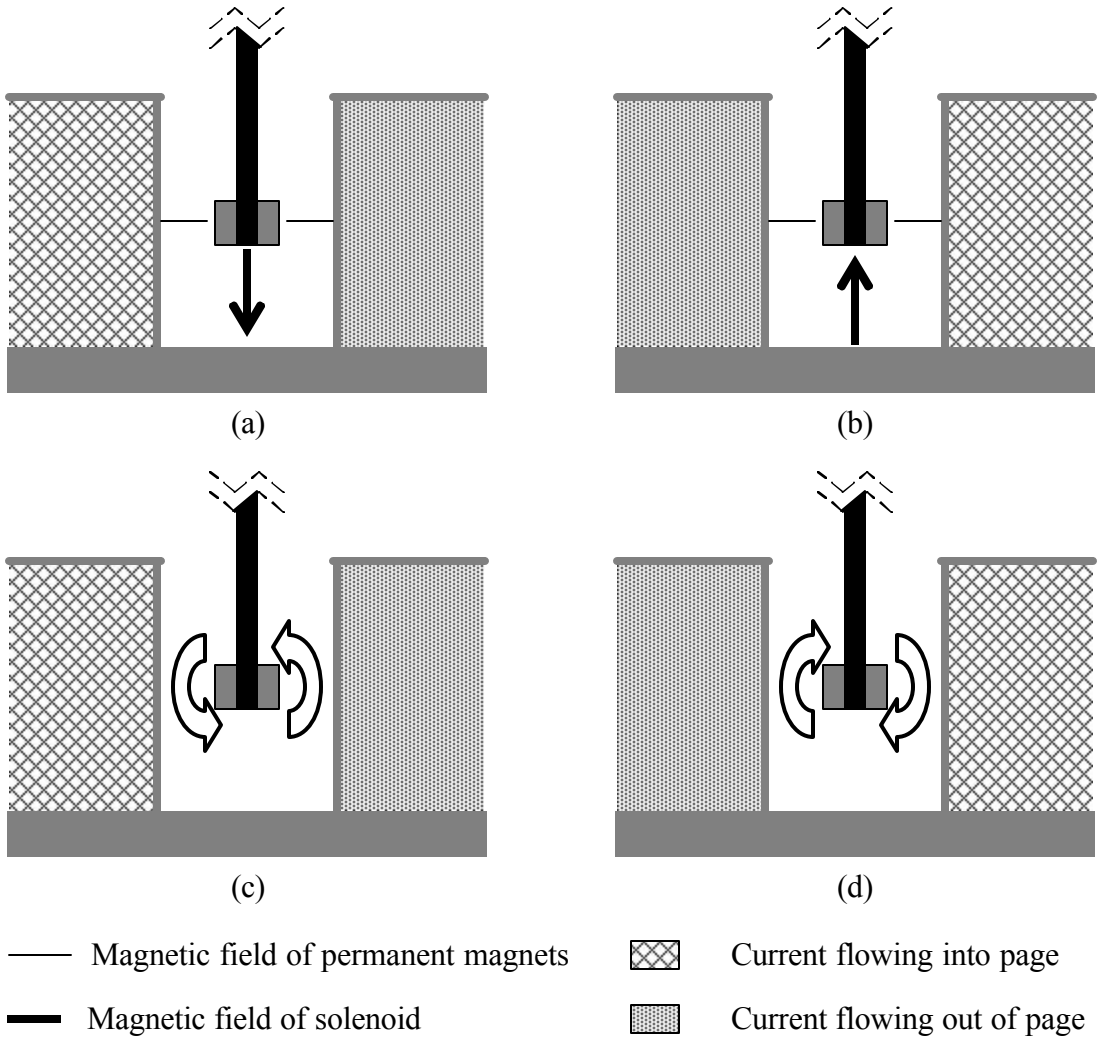

Figure 5. Alternating Excitation of the Beam (a) and (b) Magnetic fields of coil and permanent magnets; (c) and (d) Alternating moment corresponding to magnetic field interactions in (a) and (b)

coil magnetic field reverses direction as well and the permanent magnets experience an applied moment in the opposite direction. The result of this alternating, external magnetic field is a torque that "excites the vibration modes of the beam without exciting the rigid body pendulum motion of the beam" [7].

An alternative method was attempted by the TEFF. They configured the experiment as illustrated in Figure 6, hoping the attractive/repulsive force between the two magnetic fields would be enough to vibrate the beam; however, the resultant action of the beam was to swing back and forth. As such, the rigid body pendulum motion of the beam was observed as opposed to the desired vibratory motion.

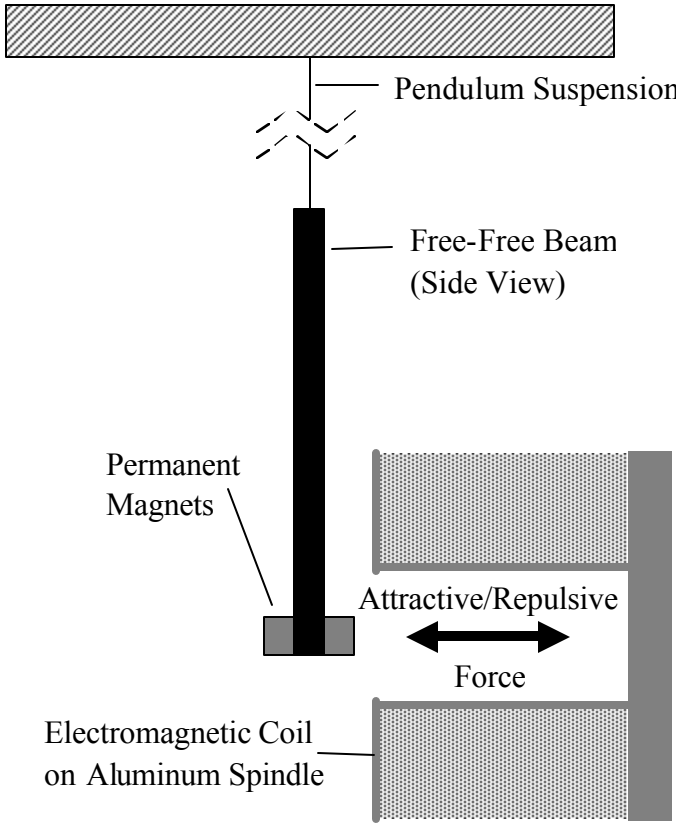

Figure 6. Alternate Configuration of the TEFF System

Electromagnetic Torque Prediction

As stated previously, the configuration and the use of the system was fairly simple for the TEFF's early damping experiments. It provides an effective tool for observing and modeling damping characteristics for bare and coated beams; however, not enough is

understood about the electromagnetic torque to analyze and predict when fatigue will occur under high cycle conditions.

An Electromagnetic Tool for Damping and Fatigue Analysis

Although the system has been used to characterize the effectiveness of damping treatments, the system is not yet fully understood, which leads to the thrust of this research and experimentation effort. The purpose is threefold: (1) Develop an equation to predict the magnetic field produced by an electromagnetic coil, (2) Develop an equation for predicting the torque exerted on the beam, and (3) Experimentally validate the accuracy of these equations.

Develop an Equation to Predict the Magnetic Field Produced by an Electromagnetic Coil

Magnets and electromagnetic coils are used daily with numerous applications. From refrigerator doors to electric car locks to computers, many of the devices in our homes work through the "magic" of electromagnetics. While these applications are widely used and understood, it is somewhat difficult to accurately predict the magnetic field of an electromagnetic coil, build it, and validate the prediction.

Electromagnet design, although quite complex, is rooted in one of the fundamental laws of electromagnetics—the Biot-Savart Law. The Biot-Savart Law is electromagnetics in its most basic form, but it does not easily translate to predicting the magnetic field of a coil. Furthermore, because all magnetics essentially occur on the

atomic/molecular level, slight variations in material composition can impact the magnetic field in many ways.

The Biot-Savart Law simply states a wire carrying a steady current I induces a magnetic field $d\vec{B}$ at a point P associated with a current element $d\vec{s}$ (see Figure 7) with the following properties [14]:

1. The vector $d\vec{B}$ is perpendicular to both $d\vec{s}$ (which is in the direction of the current) and to the unit vector $\hat{r}$.

2. The magnitude of $d\vec{B}$ is inversely proportional to r^2.

3. The magnitude of $d\vec{B}$ is proportional to the current and to the length $d\vec{s}$ of the element.

4. The magnitude of $d\vec{B}$ is proportional to the angle between $d\vec{s}$ and $\hat{r}$.

Equation 1 gives the mathematical representation of this law [14]:

$$d\vec{B} = k_m \frac{I \cdot d\vec{s} \times \hat{r}}{r^2} \tag{1}$$

where

$d\vec{B}$ = differential magnetic field strength at a distance *r* from the wire (T)

$$k_m = \frac{m_o}{4p} = 10^{-7} \frac{Wb}{A \cdot m}, \text{ a constant}$$

m_o = permeability of free space (vacuum) $= 4p \times 10^{-7} \frac{Wb}{A \cdot m}$

I = current (Amps)

$d\vec{s}$ = differential length element along the wire in the direction of the current

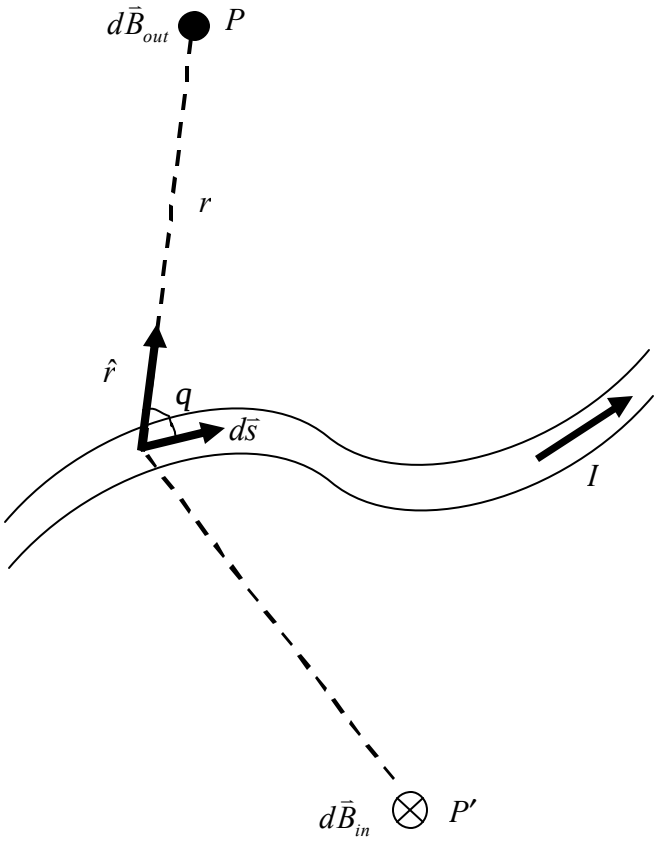

Figure 7. Magnetic Field $d\vec{B}$ at a Point P Due to a Current Element $d\vec{s}$; the field is out of the paper at P and into the paper at P' [14]

As stated above, $d\vec{B}$ represents a differential element of the magnetic field. The total magnetic field of a finite length conductor at P is found by summing the $d\vec{B}$ contributions from each current element, $d\vec{s}$, along the length of the conductor; the magnetic field lines at any distance from the conductor can be visualized as concentric rings of equal magnetic field magnitude, decreasing in magnitude as the distance from the conductor increases (see Figure 8). The result is a rotating magnetic field about the wire throughout the wire's entire length; the direction of rotation can be easily determined with the right hand rule (thumb pointing in the direction of current flow).

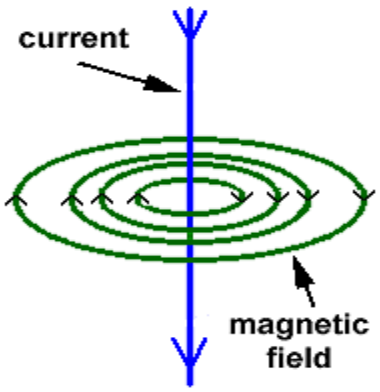

Figure 8. Magnetic Field Rotating Around a Wire (see Figure 7); magnetic field decreases as distance from the wire increases [15]

With the Biot-Savart Law, the magnetic field at any distance from a wire can be calculated; however, the key is how the magnetic field rotates about the wire. If the wire shown in Figure 8 is wrapped around an air core, referred to as a solenoid and illustrated in Figure 9, the magnetic field concentrates along the solenoid's longitudinal axis due to the additive effect of each turn of wire [15]. Infinitely long (length >> radius) solenoids are capable of achieving highly uniform magnetic fields [14].

While the field of the infinitely long solenoid is uniform, as length and radius become closer, the uniformity diminishes, but not enough to significantly impact the performance of the solenoid [13]. Since the field remains uniform, the strength of the magnetic field must be considered. As discovered by Jones, et al [7], the solenoid creates a magnetic field strong enough to vibrate the beam, but is this field strong enough to fatigue the specimen? Yes, but over long durations of time, on the order of hours [30]. It is necessary to reduce this time to minutes in order to fatigue the specimen in 10^6 cycles. The torque function is characterized as follows: $t = A\sin wt$ (A is the amplitude of the function, w is the frequency, and t is the time). For a given frequency,

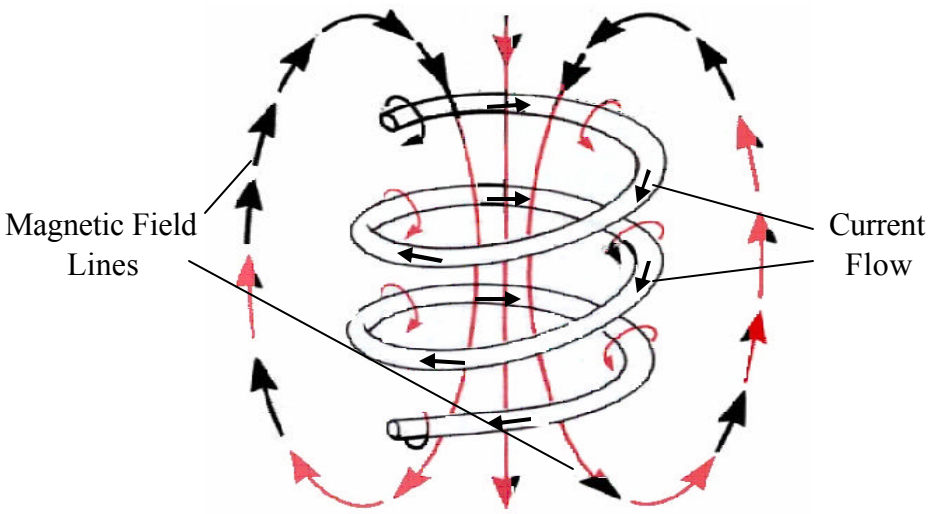

Figure 9. Coiled Wire Increases Magnetic Field (see Figures 7 and 8) [17]

the larger the amplitude, the larger the torque. The larger the torque, the larger the maximum strain-stress. The larger the maximum strain-stress, the quicker the specimen fatigues. If a beam vibrates at 1,000 Hz with a large enough torque amplitude, it should take approximately 16 minutes to fatigue the specimen in 10^6 cycles; up to this point, the TEFF's coil has not created large enough magnetic field magnitudes to create a torque amplitude strong enough to fatigue a specimen in 16 minutes. As such, a higher magnitude magnetic field must be created to achieve 16 minutes to fatigue; the air core coil alone cannot reach the desired magnetic field strengths, but with the insertion of a ferromagnetic core into the coil, the desired magnetic field strengths, and torques, are possible. Insertion of a ferromagnetic core can produce magnetizations sometimes orders of magnitude greater than the applied field [18]. This increase in magnetic field makes it possible to torque the specimen at high enough amplitude to fatigue it in the necessary time.

Ferromagnetic materials affect the magnetic field at the atomic level [19]. The ordering of electron spins in ferromagnetic materials leads to the formation of regions, called magnetic domains, where magnetic moments are aligned within the material. There is a degree of magnetization within each individual domain, but the domains are randomly oriented with respect to each other. By applying an external magnetic field, magnetic moments of neighboring atoms, and resultantly their domains, become locked into a rigid parallel order over a large number of atoms thereby lining up the domains in generally the same direction (see Figure 10).

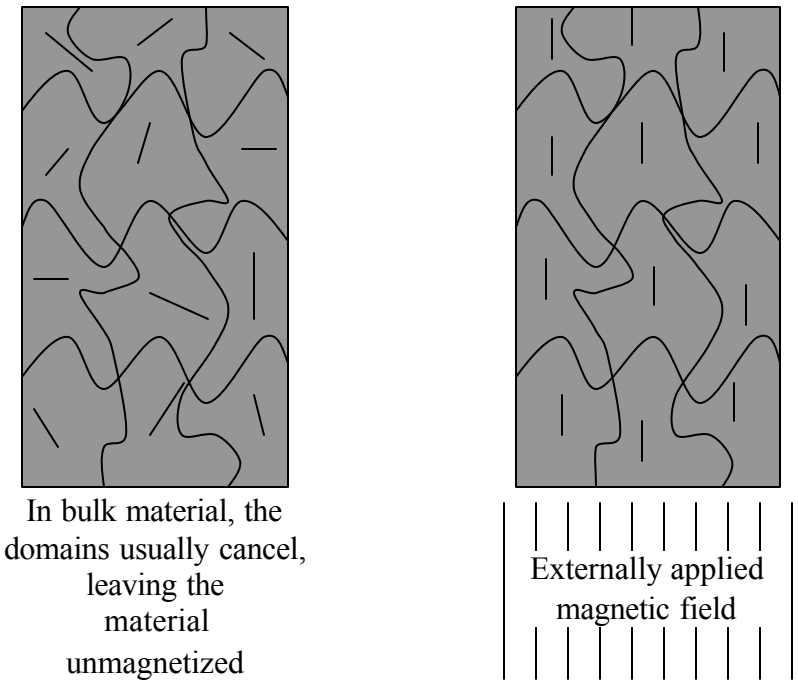

Figure 10. Magnetic Domains (the domains are the result of magnetic moments within the domain aligning with one another in generally the same direction) (a) material before externally applied magnetic field; (b) line up of the domains with the application of an external field [20]

The locked atoms grow at the expense of other atoms in the material with weaker magnetic moments thereby limiting the maximum achievable magnetic field if all the individual magnetic moments aligned. However, in ferromagnetic materials, enough of these atoms align such that the effect is to greatly intensify the magnetic field. An external field of .0002 T can produce a field of about 1 T in annealed iron. The effect of the annealed iron multiplies the strength of the magnetic field by about 5000 [19]. With this type of intensification possible, it is easy to see why a ferromagnetic core is desired for applications at the TEFF. Figure 11 illustrates the difference in an air core coil and a ferromagnetic core coil as a result of the aligning of the magnetic moments and therefore the magnetic domains under the influence of an externally applied magnetic field.

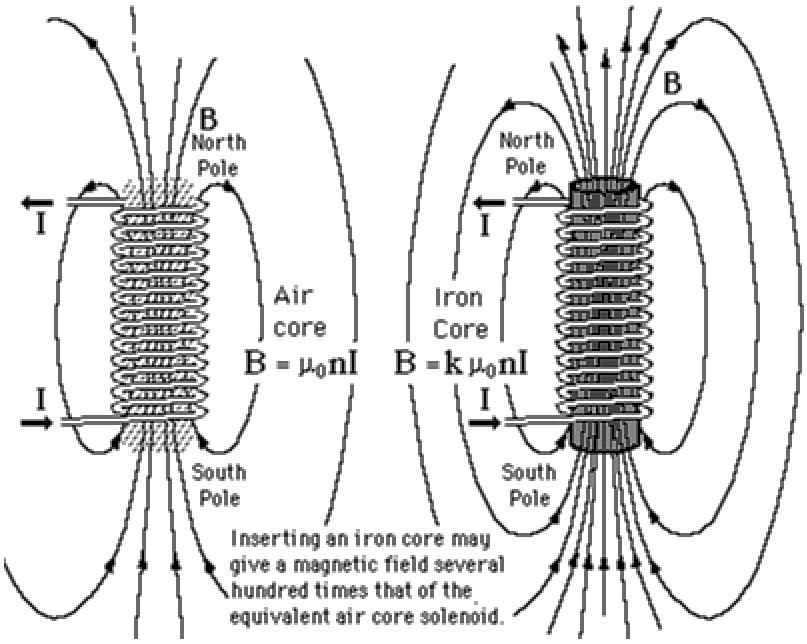

Figure 11. Magnetic Field of an Air Core vs. an Iron Core Coil [20]

The formulas for computing the strength of a coil are also shown in Figure 11. n represents the number of turns of wire per unit length (in Figure 11, there are 14 turns of wire over the length of the coil, n can be found by dividing 14 by the overall length of the coil); k represents the relative permeability (see Appendix A) of the core. When inserting a core into a hollow solenoid, the magnetic field of the solenoid is multiplied by the relative permeability of the core material. The relative permeability of the material is calculated by dividing the magnetic permeability of the substance (see Appendix A) by the permeability of free space [18]:

$$k = \frac{m}{m_o} \tag{2}$$

where

$$m = \text{magnetic permeability of the material} \left(\frac{Wb}{A \cdot m} \right)$$

Magnetic permeability is a constant of proportionality that exists between magnetic induction and magnetic field intensity. It is used to represent a material's ability to cause the magnetic field lines to move closer together or farther apart. Materials that cause the field lines to move farther apart as compared to free space are called diamagnetic. Materials that concentrate the magnetic flux lines by 1 to 10 times are called paramagnetic. Materials that exceed a concentration factor of 10 are known as ferromagnetic [16]. Most permanent magnets are made from ferromagnetic substances because of their ability to sustain a magnetic field; however, when dealing with electromagnetic coils, ferromagnetic cores are used in a wide variety of applications due

to their ability to significantly magnify the magnetic field of the coil. As such, low power, ferromagnetic core coils, can be used to create very strong magnetic fields as compared to the magnetic fields produced by an air core coil operating at the same power.

Knowing ferromagnetic cores can definitely produce high magnitude magnetic fields, the problem turns to calculating the magnitude of these fields. Figure 11 shows equations for calculating the field strengths of infinitely long solenoids and coils, but equations for finite length solenoids and coils are necessary for TEFF applications. Equation 1 gives the mathematical form of the Biot-Savart Law; through derivations discussed in Chapter 2 of this document, the equation for the magnetic field at a distance x_1 from the coil is (see Figure 12 for explanation of variables) [21]:

$$B = \frac{m_o \cdot I \cdot n}{2(R_2 - R_1)} \left[x_2 \ln \frac{\sqrt{R_2^2 + x_2^2} + R_2}{\sqrt{R_1^2 + x_2^2} + R_1} - x_1 \ln \frac{\sqrt{R_2^2 + x_1^2} + R_2}{\sqrt{R_1^2 + x_1^2} + R_1} \right] \tag{3}$$

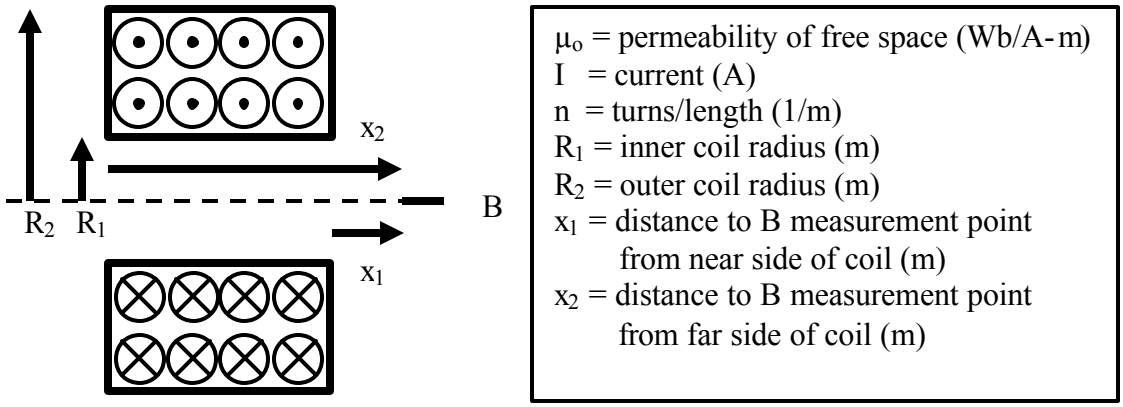

Figure 12. Variable Explanation for Finite Solenoid

Develop an Equation for Predicting the Torque Exerted on a Beam

One of the primary benefits of the TEFF setup shown in Figure 2 versus the configuration shown in Figure 6 is with the setup displayed in Figure 2, torque is exerted on the permanent magnets by the coil; in the setup shown in Figure 6, force is exerted on the magnets, not torque. While this torque is highly effective for exciting vibration in the beam, like the magnetic field of the coil, it can be a difficult commodity to accurately predict due to the variability of material composition at the atomic/molecular level.

Fortunately, an equation exists for calculating the torque exerted on a current loop when acted upon by an external magnetic field [14]:

$$\vec{\tau} = \vec{m} \times \vec{B} \tag{4}$$

where

$\vec{m}$ = magnetic dipole moment of the loop $\left(A \cdot m^2\right)$; $\perp$ to the plane of the loop

$\vec{B}$ = magnetic field strength (Teslas)

This equation is valid for any orientation of the current loop. Furthermore, it is valid for any loop shape (rectangle, circle, etc) and is applicable to electromagnetic coils as well. Once again, magnetics ultimately occur on the atomic level where atoms are true dipoles (see Appendix A). On a macro level, it can be effective to model magnetic fields as dipoles depending on the circumstances of the scenario [22]. For instance, bar magnets are regarded as magnetic dipoles, when in actuality, they are not, even though they are very accurately modeled as dipoles. Additionally, two sources [22, 24] state the accuracy of this technique is based on the distance the modeled dipole is away from the

source of the external magnetic field. All other sources mention no distance dependence with the use of this technique; the experimental plan in Chapter III discusses this concept and the assumptions made to model the permanent magnets as dipoles in further detail.

Besides verifying the accuracy of this equation, an additional problem remains when modeling the torque and magnetic dipole moment: the derivation and subsequent calculation of the magnetic dipole moment of a permanent magnet.

The magnetic dipole moment (see Appendix A) of a current loop is based on its area and the current flowing through it:

$$\vec{m} = I \cdot \vec{A} \tag{5}$$

Since there is no current applied to the magnets attached to the beam, an alternative method must be developed to calculate their magnetic dipole moment. Fortunately, permanent magnets magnetized in a single direction can be thought of as a summation of current loops. In the TEFF setup, the permanent magnets attached to the beam are cylindrical and can be considered this way, leading to Equation 6 [22]:

$$\vec{m} = \frac{\vec{B}_i \cdot V}{m_o} \tag{6}$$

where

$\vec{B}_i$ = intrinsic induction of magnet (Teslas); measured at one of the poles (either end)

V = volume of the magnets (m^3)

m_o = permeability of free space

Equation 6 is valid for any geometry where the volume can be found or calculated; furthermore, Figure 16 in Chapter II further illustrates this concept. Chapters II and III will discuss in detail the theory behind this equation and the experimental plan to validate the accuracy of Equations 4 and 6.

Experimentally Validate the Accuracy of Magnetic Field and Torque Equations

Please see Chapter III for details regarding this section; Chapter III deals entirely with the experimental plan including assumptions, setup, etc.

II. Theory

Overview

The purpose of this chapter is to develop the equations which will be used to do the following experimentally:

1. Confirm the strength of the magnetic field,
2. Test the accuracy of the magnetic dipole model of the permanent magnets, and
3. Validate the torque exerted on the permanent magnets by the coil.

Calculating the Axial Magnetic Field of a Finite Solenoid

As stated previously in Chapter I, the derivation for this calculation is rooted in the mathematical form of the Biot-Savart Law, Equation 1 (see Figure 7, p11 for explanation of variables) [14].

$$d\vec{B} = k_m \frac{I \cdot d\vec{s} \times \hat{r}}{r^2} \tag{1}$$

Axial Magnetic Field of a Circular Loop

In order to get to the equation for the axial magnetic field of a finite solenoid, a circular loop must first be considered. Consider a circular loop of wire of radius R located in the yz plane, carrying a steady current I, as in Figure 13. The field at an axial point P, a distance x from the center of the loop, is desired.

For this setup, any element $d\vec{s}$ is perpendicular to $\hat{r}$. Additionally, all elements around the loop are the same distance, *r*, from *P*, and $r^2 = x^2 + R^2$. As such the magnitude of $d\vec{B}$ induced by $d\vec{s}$ is [14:839]:

$$dB = \frac{m_o \cdot I \cdot \left| d\vec{s} \times \hat{r} \right|}{4 \cdot p \cdot r^2} = \frac{m_o \cdot I \cdot ds}{4 \cdot p \cdot \left(x^2 + R^2 \right)} \tag{7}$$

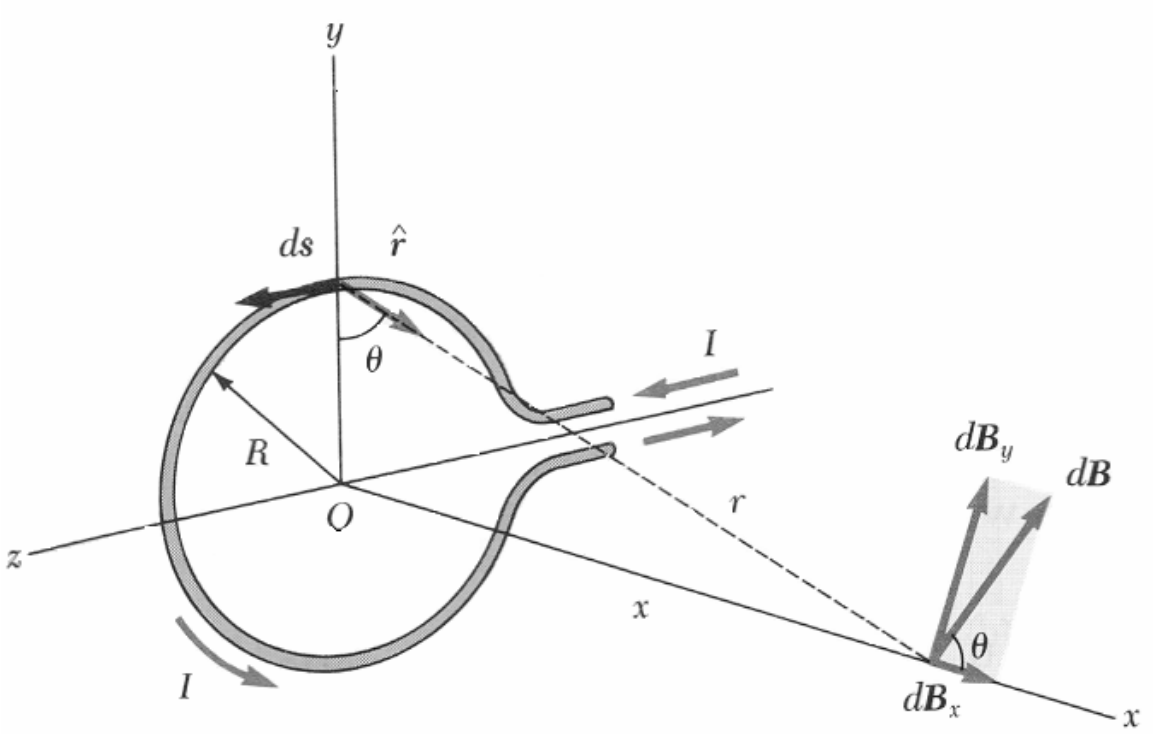

Figure 13. Magnetic Field at an Axial Point for a Current Loop [14:839]

The direction of the magnetic field $d\vec{B}$ is perpendicular to the plane formed by $d\vec{s}$ and $\hat{r}$. After resolving $d\vec{B}$ into its components, dB_x and dB_y, it is necessary to sum the contributions from each $d\vec{s}$ over the entire loop. When summing the components

dB_y over the whole loop, the result is zero. By symmetry, for every dB_y pointing in one direction, there is an equal and opposite dB_y to cancel it; the net effect is zero magnetic field perpendicular to the x-axis. Therefore, the resultant field at *P* is along the x-axis and can be found by integrating dB_x over the entire loop [14:839]:

$$B_x = \oint dB_x = \oint dB \cdot \cos q = \frac{m_o \cdot I}{4 \cdot p} \oint \frac{ds \cdot \cos q}{x^2 + R^2} \tag{8}$$

where

$$dB_x = dB \cdot \cos q$$

q, x, and *R*, are constants for all elements of the loop, and $\cos q = R/(x^2 + R^2)^{1/2}$ therefore, Equation 8 becomes [14:839]:

$$B_x = \frac{m_o \cdot I \cdot R}{4 \cdot p \cdot \left(x^2 + R^2\right)^{3/2}} \int_0^{2pR} ds = \frac{m_o \cdot I \cdot R^2}{2 \cdot \left(x^2 + R^2\right)^{3/2}} \tag{9}$$

Axial Magnetic Field of a Finite Solenoid

Knowing the equation for a circular loop is essential to the discussion of the magnetic field strength for a solenoid, but the integration thus far has been geometrical. With solenoids, integrating with regard to infinitesimal magnitudes of geometry does not satisfy the equation; as such the integration must be turned to a non-geometrical entity of infinitesimal magnitude—the current [23] (for a complete derivation with respect to dimensionality (units) see Appendix B).

By integrating current loops of infinitesimal magnitude, *dI*, it is possible to accurately determine the field strength axially along the coil. Now, attention must be turned to how each *dI* contributes to dB_x and to deriving the relationship between a non-geometrical entity, *dI*, and known geometrical entities, *dx* and *dR* [13]. From Equation 9 and the relationship between *dI* and dB_x:

$$B = \int dB_x = \frac{m_o \cdot R^2}{2\left(x^2 + R^2\right)^{3/2}} \int dI \tag{10}$$

To do this, picture a slice taken longitudinally through the center of the solenoid as illustrated in Figure 13.

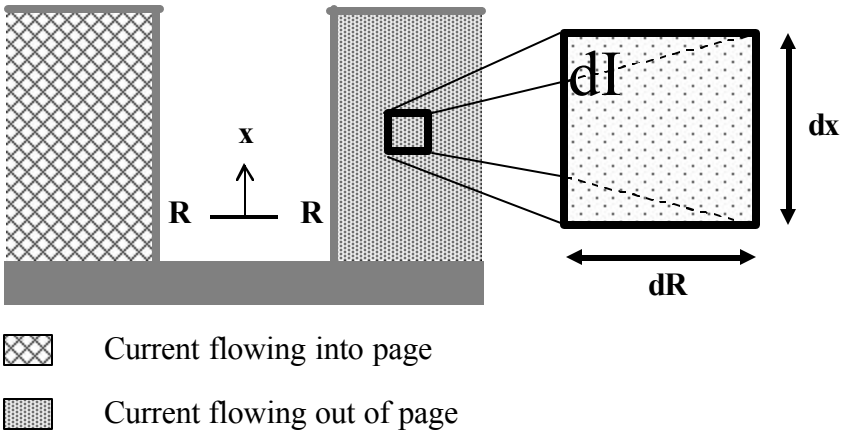

Figure 14. Infinitesimally Small Box with Current Flowing Through It

The box with dimensions *dx* and *dR* represents an infinitesimal geometry with current, *dI*, flowing through it.

dI is the total current flowing through that infinitesimally small box, but the current density, J (A/m^2), now becomes the preferred quantity because

$$dI = J \cdot dx \cdot dR \tag{11}$$

substituting Equation 11 into Equation 10,

$$B = \frac{m_o \cdot R^2}{2\left(x^2 + R^2\right)^{3/2}} \int dI = m_o \cdot J \int_{R_1}^{R_2} \int_{x_1}^{x_2} \frac{R^2}{2\left(x^2 + R^2\right)^{3/2}} dx \cdot dR \tag{12}$$

However, current density, *J*, for a solenoid is based on the number of "circular loops" (see Figure13), or wires, contained in the solenoid cross section, the current flowing through each wire, and the cross sectional area (see Figure 15).

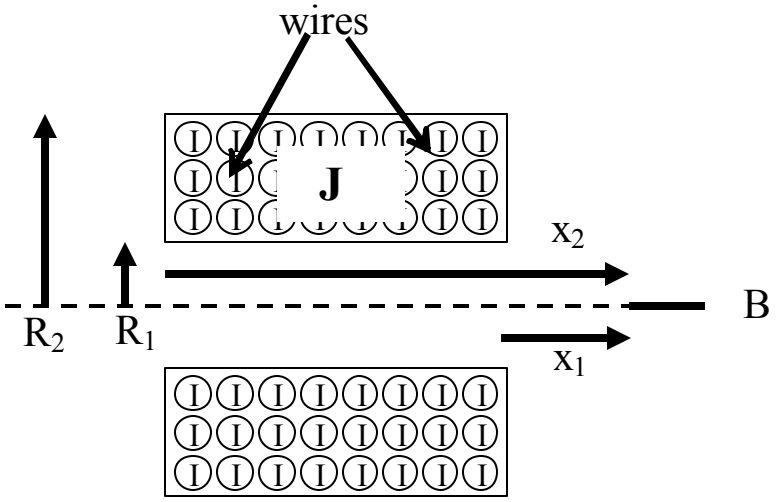

Figure 15. Longitudinal Cross Section of Solenoid

Based on the geometry represented in Figure 15, the equation to calculate current density is:

$$J = \frac{N \cdot I}{A} \tag{13}$$

where

N = number of turns of wire

I = current (Amps)

$A = (R_2 - R_1)(x_2 - x_1)$ = cross section area (m^2)

An important thing to note is $A \neq 2(R_2 - R_1)(x_2 - x_1)$; in essence, A is calculated for one side of the coil. This is a direct result of treating each turn of wire as a circular loop (see Figure 13). If A is calculated incorrectly ($A = 2(R_2 - R_1)(x_2 - x_1)$), each turn of wire would be counted twice leading to an inaccurate calculation of current density and thus magnetic field. Furthermore, since N, I, and A are all constants, J is a constant as well and belongs outside the integrand.

Substituting Equation 13 into Equation 12 yields:

$$B = \frac{m_o \cdot N \cdot I}{(R_2 - R_1)(x_2 - x_1)} \int_{R_1}^{R_2} \int_{x_1}^{x_2} \frac{R^2}{2(x^2 + R^2)^{3/2}} dx \cdot dR \tag{14}$$

Accomplishing the integration with respect to x gives [14:A.25, 24]:

$$B = \frac{m_o \cdot N \cdot I}{(R_2 - R_1)(x_2 - x_1)} \int_{R_1}^{R_2} \left[\frac{x_2}{\sqrt{x_2^2 + R^2}} - \frac{x_1}{\sqrt{x_1^2 + R^2}} \right] dR \tag{15}$$

Finally, substituting $n = \frac{N}{x_2 - x_1}$ (turns/length) and integrating with respect to R results in Equation 3 as discussed in Chapter 1 [14:A.25, 21]:

$$B = \frac{m_o \cdot I \cdot n}{2(R_2 - R_1)} \left[x_2 \ln \frac{\sqrt{R_2^2 + x_2^2} + R_2}{\sqrt{R_1^2 + x_2^2} + R_1} - x_1 \ln \frac{\sqrt{R_2^2 + x_1^2} + R_2}{\sqrt{R_1^2 + x_1^2} + R_1} \right] \tag{3}$$

Modeling Permanent Magnets as Magnetic Dipoles

In the overview of this chapter, three experimental efforts are listed for the thrust of this research effort. While the first (confirm the strength of the magnetic field) is verified with a gaussmeter, the second and third items are more difficult to confirm. Although moment can be measured in various ways, there is no way to measure the magnetic dipole of the permanent magnets in the TEFF setup for several reasons.

First, the magnetic dipole moment equation (Equation 6) is based on the magnet being a large distance (at least 5 times the largest dimension of the magnet) away from the external magnetic field [22, 25]. Second, Equation 6 is used for calculating the magnetic dipole moment of one magnet, where the beam has two magnets attached to opposite sides. Although Chapter 3 will go into more detail about the experiment, the assumption is the magnets can be modeled as a true dipole at close distances if a scaling factor is used; the scaling factor will be a function of the percentage volume difference between a true dipole (see Appendix A) and the modeled dipole to compensate for the close distance to the coil and the effect of the beam spacer between the magnets (see Figures 16 and 17) [13]. Therefore, Equation 6 must be modified as shown:

$$\vec{m} = K \cdot \frac{\vec{B}_i \cdot V}{m_o} \tag{16}$$

where K = percentage volume difference (see Figure 16) and $V = p \cdot r^2 \cdot l$.

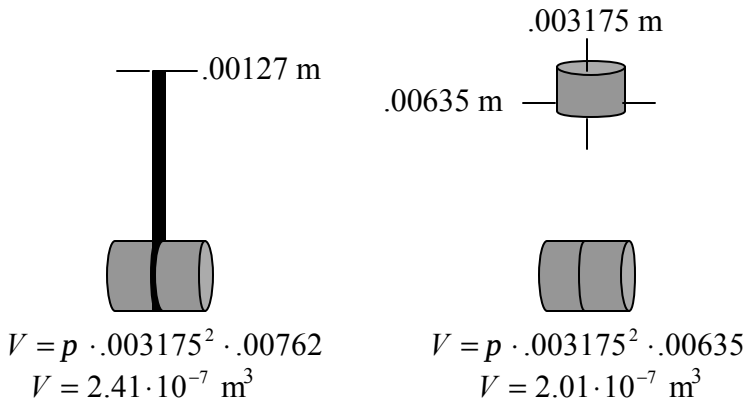

Figure 16. Volume of Magnets on Beam vs. Two Back to Back Magnets (actual dimensions of magnets and beam are used)

From the values in Figure 16 , $K = \frac{2.01 \cdot 10^{-7}}{2.41 \cdot 10^{-7}} = 0.83\overline{3}$.

Figure 16 gives the volumetric picture necessary to calculate K for Equation 6, but it does not adequately depict what is happening to the magnetic field lines when the beam is between the two magnets. Ideally, when two magnets, or more, are back to back, they act as one large magnet; this happens as a result of the linking of their magnetic field lines (see Figure 17). However, in the TEFF setup, the two magnets are not back to back; subsequently, the magnetic field lines from one magnet will begin to diverge before they link with the converging magnetic field lines of the second magnet (see Figure 18). The result is two dipoles remain; however, as the distance between the two dipoles and the source of the external magnetic field approaches infinity, they will appear as a single dipole as the two dipoles mesh into one (see Figure 19) [22].

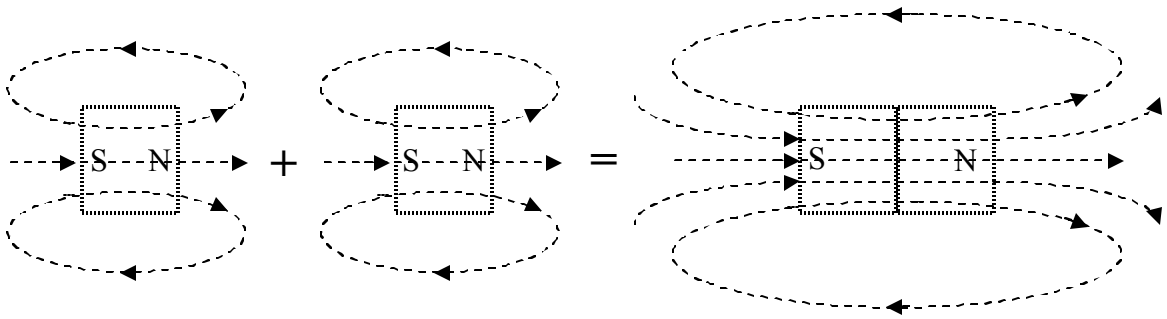

Figure 17. The Additive Effect of Placing Two Magnets Back to Back

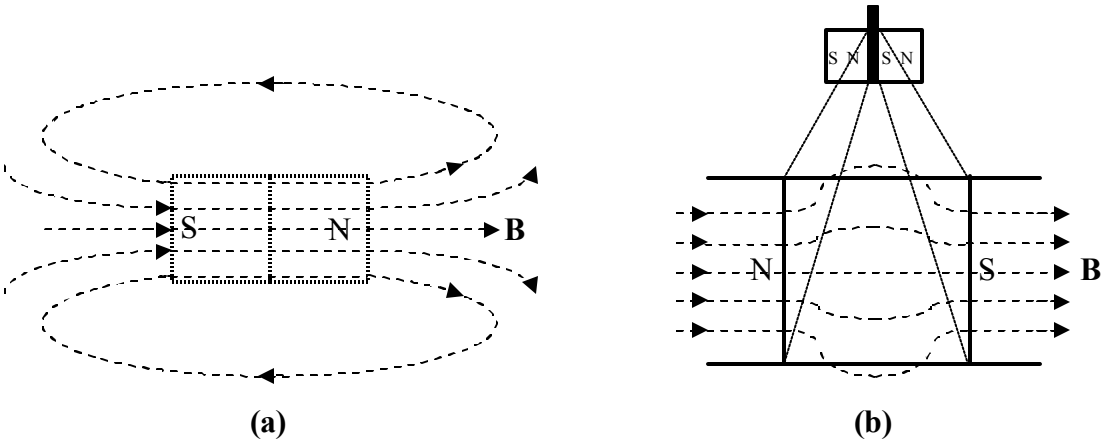

Figure 18. The Effect of a Beam Spacer on Magnetic Field Lines
(a) no spacer vs. (b) beam spacer

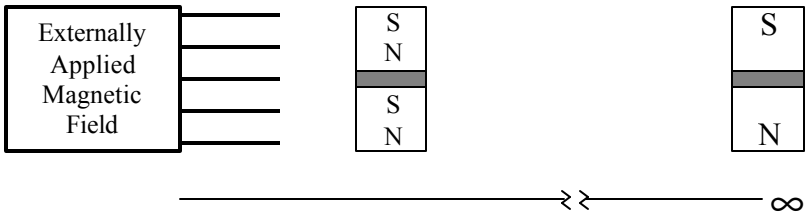

Figure 19. Increasing Distance Affects Magnetic Dipole;
two magnets with a spacer at close distance vs. the same magnets at infinity

Bearing these assumptions and keeping Figures 17 through 19 in mind, the derivation of the magnetic dipole moment is the next task. As discussed in Chapter 1, the permanent magnets attached to the beam can be treated as a summation of current loops. Hence, the torques on a magnetic dipole in a steady magnetic field are identical to those on an infinitesimal current loop with the same magnetic dipole moment [25:9].

In order to discuss the magnetic dipole moment of a current loop, the torque on the loop must first be derived from the Lorentz force law [25:9]:

$$d\vec{F} = I \cdot d\vec{l} \times \vec{B} \tag{17}$$

where $d\vec{F}$ is the infinitesimal force acting on an infinitesimal length of conductor, $d\vec{l}$, in a steady, external magnetic field, $\vec{B}$ (see Figure 20).

When the force is integrated and multiplied by the position vector, torque is calculated as follows:

$$\vec{\tau} = I \oint \left[\vec{r} \times \left(d\vec{l} \times \vec{B} \right) \right] \tag{18}$$

where $\vec{r}$ is the position vector of $d\vec{l}$

Substituting for $\vec{r} \times \left(d\vec{l} \times \vec{B} \right) = d\vec{l} \left(\vec{r} \bullet \vec{B} \right) - \vec{B} \left(\vec{r} \bullet d\vec{l} \right)$ yields:

$$\vec{\tau} = I \left[\oint \left(\vec{r} \bullet \vec{B} \right) d\vec{l} - \vec{B} \oint \vec{r} \bullet d\vec{l} \right] \tag{19}$$

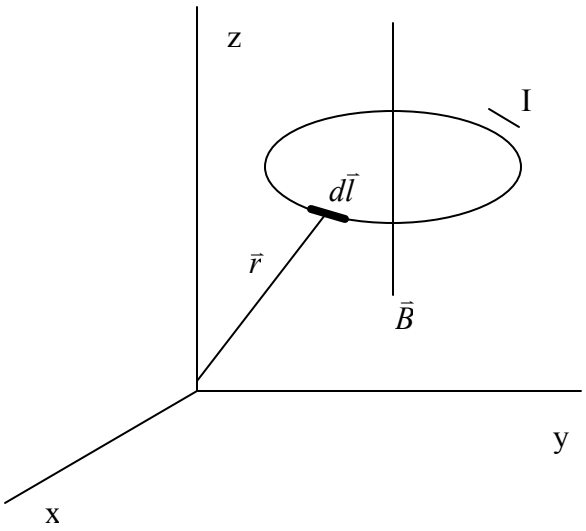

Figure 20. Plane Conductor Loop in Uniform Steady Magnetic Field

Groom expands Equation 19 so the line integrals can be transformed into surface integrals [25:9].

$$\vec{t} = I\left\{\int_s \left[d\vec{A}\times\nabla\left(\vec{r}\bullet\vec{B}\right)\right] - \vec{B}\int_s \left(\nabla\times\vec{r}\right)\bullet d\vec{A}\right\} \tag{20}$$

where $d\vec{A}$ is a differential area whose direction is normal to the plane of the current loop (in the sense of the right hand rule relative to the direction of the current)

Since $\nabla\times\vec{r} = 0$ and $\nabla\left(\vec{r}\bullet\vec{B}\right) = \vec{B}$ for constant $\vec{B}$, Equation 20 simplifies to [25:9]:

$$\vec{t} = I\int_s \left(d\vec{A}\times\vec{B}\right) \tag{21}$$

evaluating the integral results in

$$\vec{\tau} = I \cdot \vec{A} \times \vec{B} \tag{22}$$

An infinitesimal current loop can be defined by letting $\vec{A}$ go toward zero and I go toward infinity, keeping $I \cdot \vec{A}$ finite. $I \cdot \vec{A}$ is called the magnetic dipole moment of the current loop and defines $\vec{m}$ in Equation 5 as first introduced in chapter I, $\vec{m} = I \cdot \vec{A}$. Substituting $\vec{m}$ into Equation 22 results in Equation 4, $\vec{\tau} = \vec{m} \times \vec{B}$. The torque, $\vec{\tau}$, acts on the current loop in a direction to align the magnetic dipole moment, $\vec{m}$, with the external magnetic field, $\vec{B}$.

Knowing the theory behind the magnetic dipole moment of a current loop, the magnetic dipole moment of a permanent magnet follows from this theoretical assumption: a permanent magnet of a given volume, V, consists of a large number of uniformly distributed permanent magnet dipoles with incremental volume dV which are oriented in the same direction (see Figure 10) [25:10].

Each incremental dV also has an associated magnetic dipole moment, $d\vec{m}$. The magnetic moment per unit volume, magnetization ($\vec{M}$) (see Appendix A), can be calculated using the following Equation [25:10]:

$$\vec{M} = \frac{d\vec{m}}{dV} \tag{23}$$

where $\vec{M}$ is measured in units of A/m

The total magnetic moment for a permanent magnet can then be calculated when the integration is evaluated over the volume of the permanent magnet, and the magnet is uniformly magnetized over its volume ($\vec{M}$ is constant) [25:10].

$$\vec{m} = \int_V \vec{M} \cdot dV = \vec{M} \cdot V \tag{24}$$

The magnetization can alternatively be calculated with the magnetic field, $\vec{B}$, of the permanent magnet and the permeability of free space, m_o, as follows: $\vec{M} = \vec{B}/m_o$. Substituting for $\vec{M}$ in Equation 24 gives the calculation for the magnetic dipole moment as shown in earlier.

$$\vec{m} = \frac{\vec{B}_i \cdot V}{m_o} \tag{6}$$

As stated earlier, there is no direct way to measure magnetic dipole moment; therefore, there is no direct way to validate Equations 6 and 16. However, these equations are based on values that can be calculated from the magnet's dimensions (volume) or measured with a gaussmeter (magnetic field). As such, the only way to verify the magnetic dipole model is by measuring the torques for various currents, cores, and distances and comparing those values to calculated torques from Equations 3, 4, and 6—this is the basis of the experiment introduced in Chapter III.

III. Design of Experiment

Overview

In this chapter, the development of the experimental design will be discussed, beginning with the setup of the experiment and concluding with the comparison of experimental and calculated results.

Experimental Setup

The fundamental emphasis of this thesis is to verify and validate various electromagnetic equations under a system of boundary conditions and assumptions. Jones managed to build a functionally sound device with excellent initial results for damping treatments [7]; however, Jones' design does not easily present itself to the task of experimentally validating the equations derived in Chapter II.

First, the alternating current necessary to excite vibration in the beam makes it difficult to measure the magnetic field created by the coil.

Additionally, although it is widely understood the moment setup displayed in Figure 2 is far better at exciting the beam than the force setup in Figure 6, there is no direct way to measure the moment transferred to the beam from the permanent magnets.

Finally, the existing TEFF setup does not have the capability to generate currents in excess of approximately 8 amps. With this current limitation present, the magnetic field is capped, and therefore moments strong enough to fatigue a specimen are difficult to achieve.

As a result of the reasons listed above, the TEFF setup had to be changed significantly to create a situation where the torque on the magnets can be measured, which leads to one of the primary assumptions of this experiment: the torque exerted on the permanent magnets is directly transferred to the beam with no losses, or at least no significant losses.

To keep this assumption intact, the fastening of the magnets to the beam becomes a fairly critical issue. In both the Jones setup and the setup for this thesis, a stiff epoxy is used to attach the magnets. If a flexible epoxy is used, some of the torque will be transferred to, and subsequently absorbed by, the epoxy. With the stiff epoxy, the beam and the magnets will be treated as one rigid body thereby creating a condition where all the torque (no significant losses) gets transferred directly to the beam as a bending moment.

In response to the inability to directly measure the torque on the magnets, a scale/fulcrum configuration will be used. Initially, the idea was to pin the beam at its center of mass and measure the moment with a weight-bearing bucket, as shown in Figure 21. While this configuration is possible, it is not practical. The size of the beam (4.5 in x .5 in x .05 in, 11.43 cm x 1.27 cm x 0.127 cm) does not lend itself to ease of use. Furthermore, it is difficult to attach a frictionless pivot at the fulcrum point. Finally, the length of the beam limits its ability as an effective moment arm.

To deal with the limitations of the setup in Figure 21, another setup was used to measure the moment. A wooden rod (wood is not magnetic and will not be affected by the coil's magnetic field) of 45.72 cm was used to "hold" the beam and magnets (see Figure 22). With this configuration, a small hole was drilled in the rod to serve as the

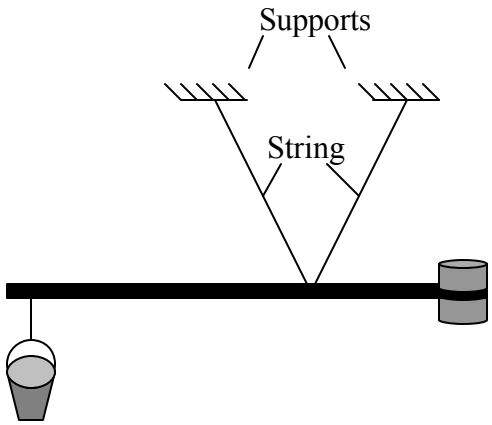

Figure 21. Initial Experimental Setup

fulcrum point. A notch was cut into one end where the beam is inserted; once inserted, the beam is tightly wrapped to make it rigid with the wooden rod. Finally, a level was placed on the beam to determine its equilibrium position.

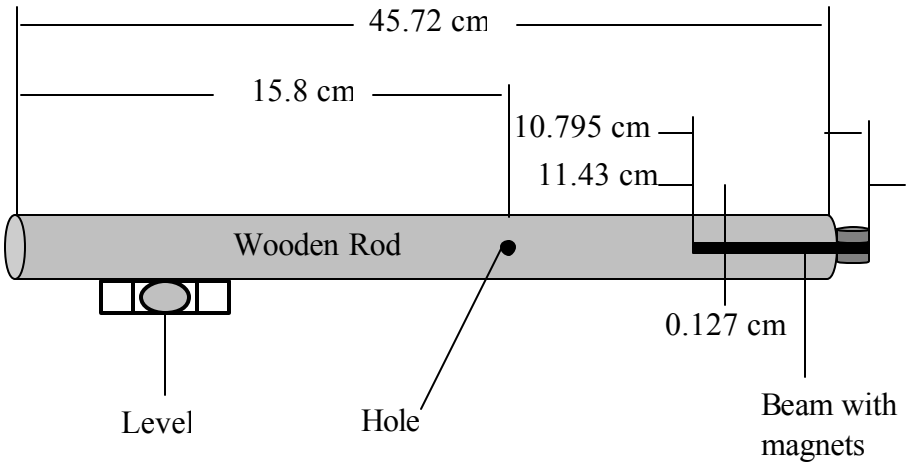

Figure 22. Experimental Configuration of Wooden Rod with Inserted Beam

With this arrangement, a stiff wire is run through the hole to serve as the fulcrum point. The wire is thin enough to provide a "near-frictionless" interface with the rod and strong enough to withstand the loads placed on it.

Another significant change is in the Jones setup (see Figure 2) the beam is suspended over the coil; the coil's magnetic field lines are vertical. In the setup for this experiment, the coil is placed on its side; its magnetic field lines are horizontal.

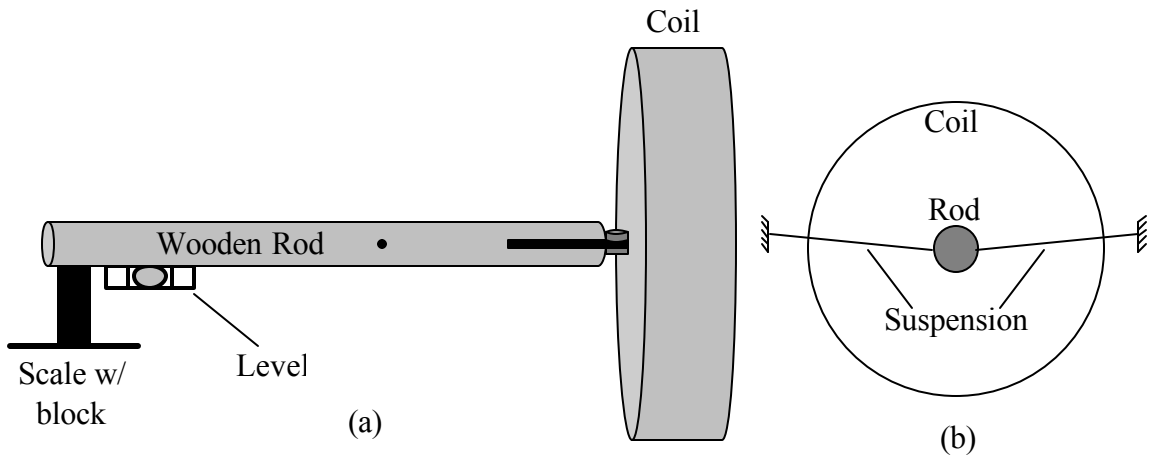

Figure 23. Experimental Configuration of Coil and Rod (a) side view; (b) end view

An additional change involved how to measure the torque. The first idea was to attach a bucket similar to the bucket in Figure 21, but the problem was, depending on the magnitude of the magnetic field, the bucket wasn't big enough to hold an adequate weight to counterbalance the torque. Consequently, a scale with a block on it was placed under the rod until the rod was level.

The final change involved the application of a direct current (DC) (see Appendix A) instead of an alternating current (AC). This current was applied with an HP-6268B power supply. As stated previously in this chapter, an alternating current makes it extremely difficult to measure and verify the moment on the beam; with DC, the beam only deflects in one direction, as opposed to alternating directions with an AC source.

Moreover, when applying a direct current, the current applied is the value used in the calculation of the magnetic field from Equation 3. When using an alternating current, the root mean square (RMS) (see Appendix A) of the applied current must be used due to the inductance of the electromagnet. The AC flow is reduced compared to a DC flow of the same value by a reduction equal to the RMS value of the AC current feeding the coil [26].

Experimental Steps

With the configuration of the experiment in mind, it is necessary to introduce the steps of the experiment. All experimental results will be covered in Chapter IV.

Step 1. Design Electromagnet.

The design of an electromagnet can be a difficult task. There are many questions to keep in mind when designing the coil. What will the core be made of; how big will the wire have to be to handle the current; etc. Fortunately, www.my.execpc.com/~rhoadley/magelect gives an excellent step by step guide to winding a coil, and the issues which need to be figured out prior to starting construction of the device [26]. For this research, the coil provided by the TEFF was previously designed and built by Jones [7].

For this experiment, it was desired to use the TEFF coil with three different cores where Jones worked exclusively with an air core: an air core, a nickel core, and an iron core. The reason being each core will affect the magnetic field in different ways. The air core will have no impact on the field, whereas the nickel and iron cores will significantly increase the field, with iron having the largest affect. Having three different cores gives

the ability to validate the magnetic field and torque equations under three different operating conditions.

Step 2. Obtain Rare Earth Magnets.

The rare earth magnets used for this experiment are Neodymium-Iron-Boron Grade 37 magnets with a maximum pull of 3 pounds and a maximum magnetic field of 3800 G. Rare earth magnets are highly desired for attachment to the beam for two reasons: they are much smaller than iron magnets, and their magnetic fields are much stronger. Their size is nice because they don't contribute as much mass to the beam as iron magnets with the same magnetic field would. Additionally, as Jones stated in his work [7], he was able to maintain a free-free boundary condition with modeshapes that did not significantly diverge from true free-free modeshapes. In essence, the 18% lumped mass of the magnets did not significantly impact the free-free conditions of the damping experiment.

Step 3. Prepare Beam Specimen.

The beam must be purchased at the desired size or machined from a sheet; it also must be not be a magnetic material so there is no attractive force between the beam and the coil which could potentially impact the torque measurements (the Ti-6Al-4V beam used in the experiment satisfies this condition). The beam dimensions for this experiment were chosen to be the same as the beam dimensions from the Jones setup [7]. Those dimensions are (l x w x h) 11.43 cm x 1.27 cm x 0.127 cm. Additionally, as previously discussed, the magnets must be attached to the beam with a rigid epoxy to preserve the assumption the magnets and beam act as one body.

Step 4. Prepare Wooden Rod (see Figure 22).

The wooden rod must have a notch cut in the end to hold the beam and have a hole drilled for the fulcrum point. The notch's dimensions must account for the magnets attached to the end of the beam; the magnets have a 0.635 cm diameter. Therefore, the notch must be at least 10.795 cm long and 0.127 cm thick (see Figure 22). The beam must be seated in the notch and wrapped tightly (hockey tape was used for this experiment) so the beam and the wooden rod act as one rigid body. Additionally, a level must be attached to track the equilibrium of the rod, before and after current is applied to the coil and subsequently torque is applied to the magnets. Finally, a wire must be run through the hole, and the rod must be suspended to achieve the fulcrum effect (see Figure 23).

Step 5. Obtain Gaussmeter.

While there are many gaussmeters commercially available, most do not have the capability to measure magnetic fields like those generated by the TEFF's electromagnetic coil (the TEFF's coil is capable of achieving fields in excess of 8 kG; most gaussmeters are used for ambient or residual magnetic field measurements and do not measure fields in excess of 100 G). Therefore, an MG-4D handheld gaussmeter with a standard transverse Hall probe was purchased from Walker LDJ Scientific, Inc. The standard transverse probe gives the capability to measure fields up to 20 kiloGauss (kG) with an accuracy of $\pm 1\%$. Transverse probes measure magnetic fields through the length of the probe and are typically used with permanent magnets. An additional probe was purchased, an HP-1245S Hall probe, to measure the fields of the coil. The HP-1245S is an axial probe, measuring fields perpendicular to the probe; these types of probes are

typically used with electromagnetic coils. The HP-1245S used with the MG-4D can measure fields up to
150 kG with an accuracy of $\pm$ 1.5%.

Step 6. Measure Magnetic Fields of All Magnets.

In order to validate the equations for magnetic field and torque, it is essential to get an actual measurement of the magnetic fields produced by the rare earth magnets and the coil.

The supplier of the rare earth magnets, McMaster-Carr, provided a value of 3800 gauss for the magnetic field at the poles. While this may be very close to the actual magnetic field measured by the gaussmeter, it could be off slightly due to material imperfections at the atomic/molecular level, manufacturing discrepancies, etc. Additionally, it is incumbent the measurement be obtained when the magnets are attached to opposite sides of the beam in order to determine what impact, if any, the beam, as a spacer, has on the magnetic field of the magnets (see Figure 18). These measurements are necessary to accurately calculate the magnetic dipole moment (Equation 6) of the magnets.

Furthermore, with the aim of verifying the magnetic field of the coil (Equation 3), it is essential to get an accurate magnetic field measurement from the coil for each current applied.

Finally, with accurate magnetic field measurements, it will be possible to calculate a theoretical torque on the beam for each current applied which will later be compared to the torque measured experimentally.

Step 7. Experimentally Determine Relative Permeability of Each Core.

The only core where an actual value for the relative permeability is known is the air core, whose permeability is essentially equal to m_o, the permeability of free space; however, the relative permeabilities of the nickel and iron cores are necessary to calculate their magnetic fields (see Figure 11). As stated in Chapter 1, the relative permeability, k, multiplies the magnetic field and can be calculated with Equation 2 if the magnetic permeability of the material, m, is known. The problem is the magnetic permeability of two pieces of iron can be significantly different because the value of m is not a material characteristic of iron; it depends on the previous state and treatment of the material [14:856]. For instance, a piece of annealed iron would have a different relative permeability than a piece of cast iron. So, the issue becomes one of determining the magnetic permeability of each core.

Using the gaussmeter, a measure of the magnetic field produced by the air core coil will be taken at several currents. The nickel and iron cores will then be inserted, and the magnetic field will be measured again at the same currents. The only change is the core, therefore, the relative permeability will be calculated using the magnetic field values from the air core as follows:

$$k_j = \frac{B_j}{Ba_j} \tag{25}$$

where

$j = 1..n$, with n being the number of measurements made

B_j = a magnetic field measurement of the iron or nickel core for a specific current (T)

Ba_j = a magnetic field measurement of the air core for a specific current (T)

k_j = the relative permeability for a specific current

Finally, k, the relative permeability of each core which will be used to calculate the magnetic field to be verified experimentally, will be calculated by averaging the values of all the relative permeabilities for a specific current.

Step 8. Calculate Magnetic Field of Each Core as a Function of Current.

Having experimentally determined the relative permeabilities of each core, it is time to calculate and predict the magnetic field produced by each core using Equation 3 for the air core and Equation 26 for the nickel and iron cores (see Table 1). All variables in these equations will be held constant for each core while the current is varied; these values will be compared to measurements made with the gaussmeter to validate the accuracy of using these equations to predict magnetic fields for a coil.

$$B = k \cdot \frac{m_o \cdot I \cdot n}{2(R_2 - R_1)} \left[x_2 \ln \frac{\sqrt{R_2^2 + x_2^2} + R_2}{\sqrt{R_1^2 + x_2^2} + R_1} - x_1 \ln \frac{\sqrt{R_2^2 + x_1^2} + R_2}{\sqrt{R_1^2 + x_1^2} + R_1} \right] \tag{26}$$

Table 1. Theoretical Magnetic Fields for Various Currents

Current (A)	Magnetic Field (G)		
	Air Core	Iron Core	Steel Core
5	165.63	296.04	296.63
10	331.27	592.08	593.26
15	496.9	888.11	889.89
20	662.53	1184.15	1186.53

Step 9. Calculate Magnetic Field of Each Core as a Function of Distance.

While the torque exerted on the magnets is a direct result of the magnetic field produced by the current, it is also desired to determine how the scaling factor, K, from Equation 16 (see Figure 16) will change with respect to increasing distance from the coil. Equations 6 and 26 will be used to calculate the magnetic field as x_1 and x_2 get larger (see Table 2 and Figure 24); as x_1 and x_2 get larger, the scaling factor approaches 1. The magnetic field calculations for increasing distance will then be compared to experimental results to map K's response to a larger gap between the permanent magnets and the coil.

Table 2. Theoretical Magnetic Fields for Various Distances (Current = 5 A)

Distance (m / in)	Magnetic Field (G)		
	Air Core	Iron Core	Steel Core
0.0127 / 0.5	119.3	213.18	213.61
0.0254 / 1	72.6453	129.84	130.1
0.0381 / 1.5	45.3883	81.1227	81.2853
0.0508 / 2	29.5516	52.8177	52.9235
0.0635 / 2.5	20.0581	35.8499	35.9218

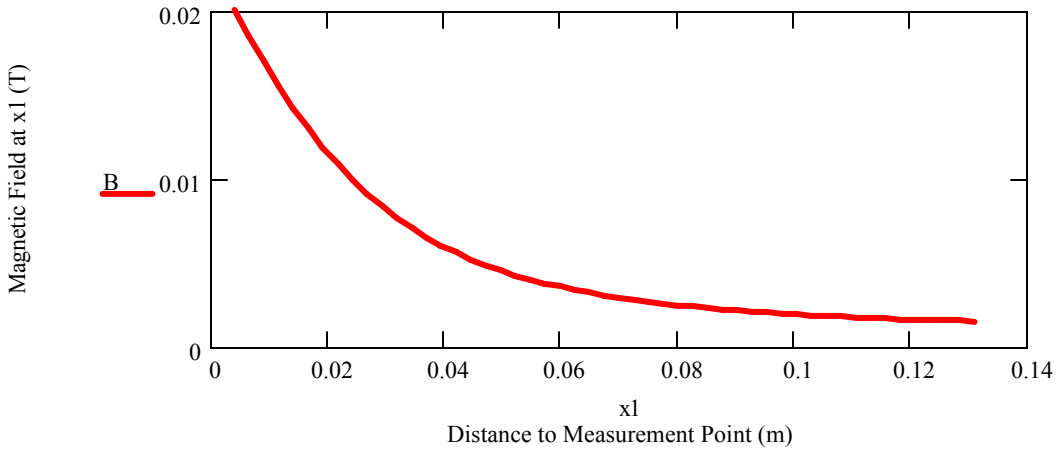

Figure 24. Magnetic Field Decreases as Distance from the Coil Increases

Step 10. Calculate Theoretical Torque.

The theoretical torque for each current and each distance will be calculated using Equation 4. The measured magnetic field values from step 6 will be used to compute this torque for compare with the experimentally measured moment.

Step 11. Measure Experimental Torque.

With all theoretical calculations complete, it is time to experimentally measure the torque on the beam. As current is applied to the electromagnet, moment will be applied to the beam which when transferred to the wooden rod will apply a force to the scale (see Figures 23 and 25). The scale is capable of measuring mass accurate to $1/1000^{th}$ of a gram. Any weight (block weight) on the scale before the torque is applied is subtracted from the displayed weight after torque application. This weight difference is then used to calculate the experimental moment using Equation 27.

$$\vec{\tau}_e = \vec{F} \times \vec{d} \tag{27}$$

where

$\vec{\tau}_e$ = experimental moment (N-m)

$\vec{F}$ = force (N)

$\vec{d}$ = moment arm distance, see Figure 22 (m)

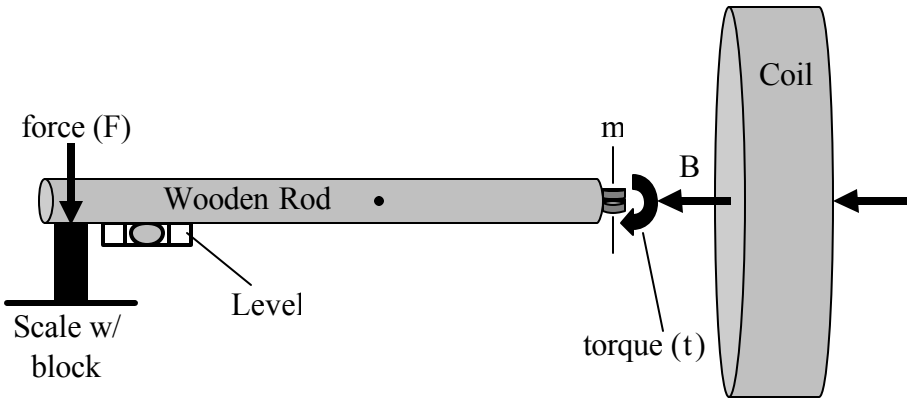

Figure 25. Moment Exerted on Beam and Subsequent Force on Scale

Step 12. Compare Values.

The last step is to compare all calculated values to all experimental values. Chapter IV addresses comparing these values and results of the experiment including verification and any modifications made to the experiment.

IV. Discussion of Results

Overview

In this chapter, the results from the experiment will be discussed. Modifications to the experiment will be addressed first. Results of the experiment will be included next, and how these experimental results compare with the theoretical results. Finally, a section covering how the TEFF can use this data will be presented. Chapter IV only presents the data obtained from the experiment and compares it to the theoretical calculations; see Chapter V for conclusions.

Modifications

The first, and most significant, modification arrived as a result of the inability to machine nickel; nickel was originally chosen because its relative permeability is typically about half that of iron. Nickel is difficult to machine because it work hardens (it hardens as it is machined); the TEFF does not have the ability to flush the nickel with coolant as it is being machined. Therefore, a piece of steel was obtained to serve as the third core. Although the steel core is mainly composed of iron, it did have a slightly higher relative permeability than the iron core, and it produced results similar to those of the iron core where uniformity of the magnetic field as it leaves the core surface is concerned. The other modification came about as a result of discovering a way to consistently measure the magnetic field with the gaussmeter probe (see Figure 26).

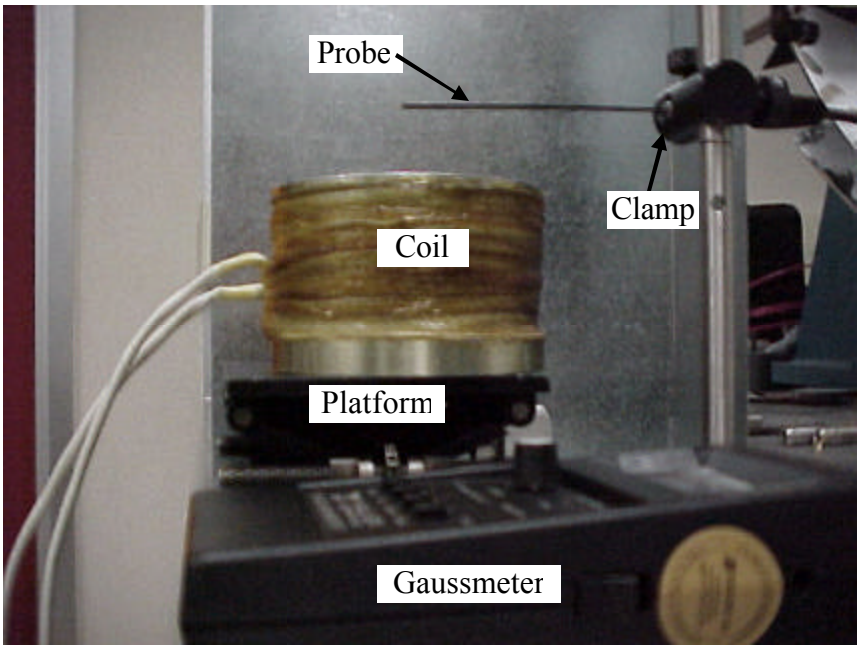

(a) Side View

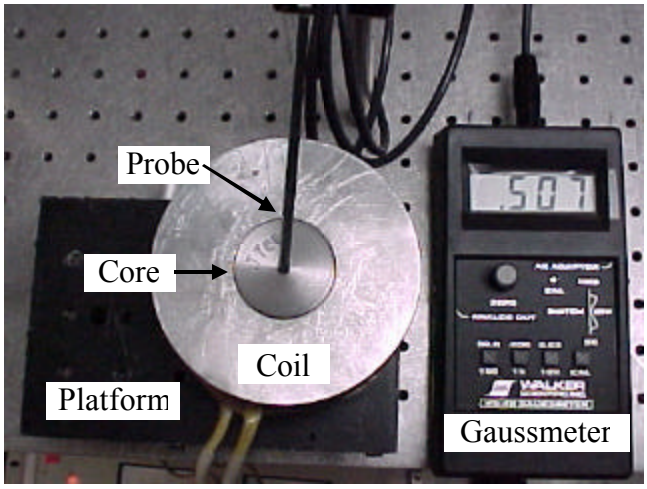

(b) Top View

Figure 26. Experimental Configuration to Measure Magnetic Field

The probe is inserted through a circular hole in the clamp which is attached to a vertical rod. The probe, being a transverse probe, measures magnetic field passing

perpendicular through its active area (see Figure 27). As such, it was clamped over the longitudinal axis of the coil to measure the magnetic field at its theoretically strongest point. Additionally, the platform (see Figure 26) has the capability to move up and down so the probe remains stationary while the coil drops away to increase the distance between the probe and the coil to consistently measure the magnetic field at increasing distances from the coil.

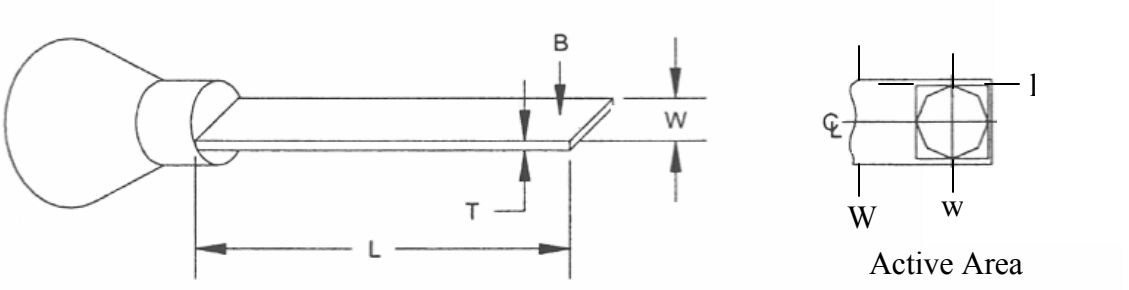

Figure 27. Transverse Hall Probe and Its Active Area (B indicates direction of the magnetic field component measured by the probe)

The final modification to the experiment was needed to keep the wooden rod "on track" as torque is applied to the permanent magnets (see Figure 28). In the ideal situation, torque is only applied around the torque axis as indicated in Figure 25; in reality, the most significant torque is applied this way. There are other torques acting all around the permanent magnets; none as strong as the previously discussed torque, but just strong enough to slightly deflect the rod in other directions. Therefore vertical rods were added to the experiment to keep the wooden rod moving in one direction in order to verify the strongest torque acting on the beam.

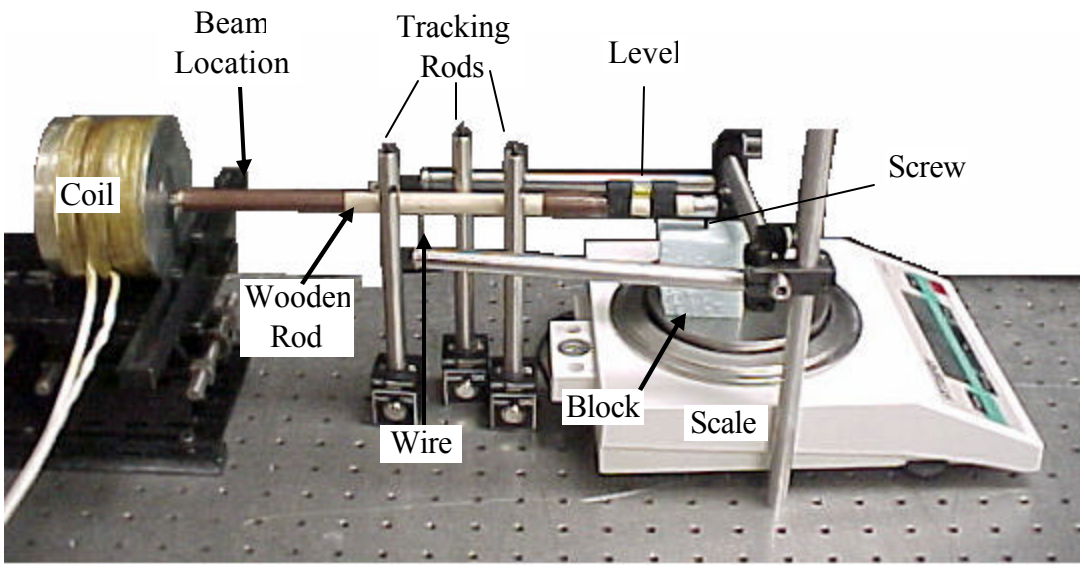

(a) Side View

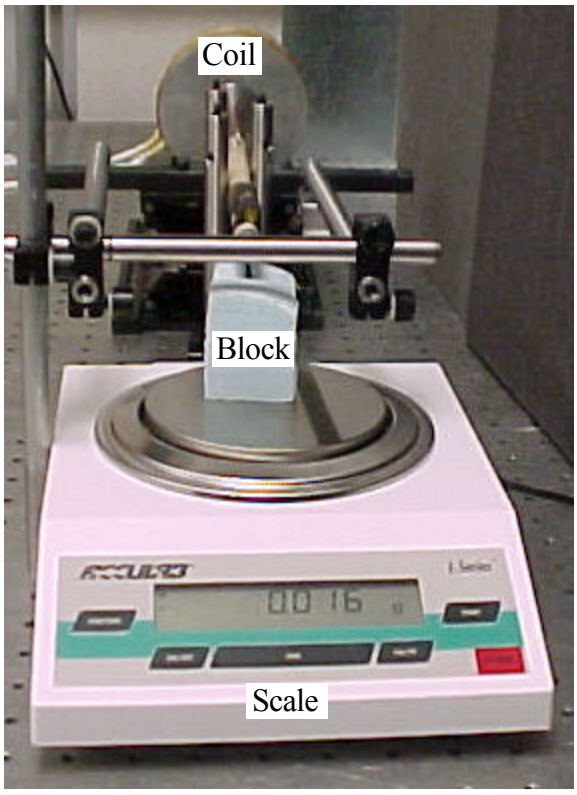

(b) End View

Figure 28. Experimental Configuration to Measure Torque

When the current is alternating, the vibratory motion of the beam is enough to keep the beam moving back and forth in one direction, but when operating under dc conditions, there is no vibratory motion to override the smaller torques. Furthermore, since the rod never actually moved from its equilibrium position, it was more susceptible to the smaller, deflecting torques than a vibrating beam would be.

In a close up of Figure 28b, a screw is protruding from the top of the block (see Figure 29). The screw was placed in the block for two reasons. First, it provided a sharp point where the torque applied from the magnets is transferred to moment in the rod and converted to equilibrium force in the screw. Second, by turning the screw, it would raise or lower the end of the wooden rod to achieve the initial equilibrium condition necessary to begin the torque measurements.

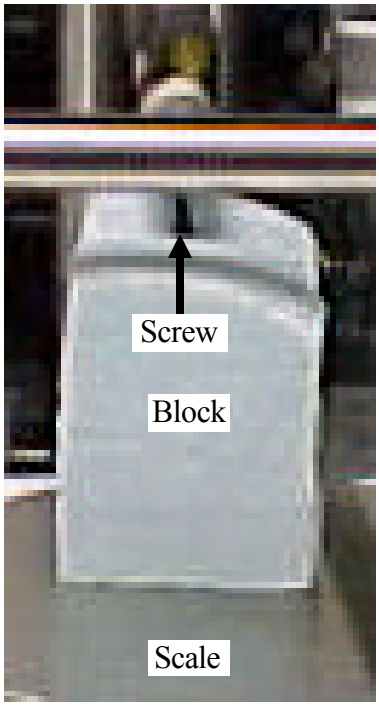

Figure 29. Screw in Block on Scale

Experimental Results

Measure Magnetic Field of All Magnets.

Using the gaussmeter, it was necessary to confirm the magnetic field of the permanent magnets. McMaster-Carr supplied a value of 3.8 kG; however, this is a maximum value. Due to inconsistencies at the atomic/molecular level, this value is an approximate value. Furthermore, it was necessary to determine the impact on the magnetic field when the two magnets are attached to opposite sides of the beam (see Figures 16 and 22). When placing two magnets of the same strength back to back, the magnetic field of the new magnet is not double the magnetic field of the two individual magnets; rather, it is just a longer magnet with a magnetic field strength comparable to the two individual magnets. For this experiment, the gaussmeter's probe was placed in contact with the magnets after they have been attached to the beam. Per the manufacturer's instructions [29:4], the probe was oriented to obtain a maximum reading; the maximum reading is the magnetic field of the magnet. On one end of the magnets, the south pole, the magnetic field was -3.18 kG; at the other end, the north pole, the magnetic field was 3.22 kG. Averaging these two measurements yields a value of ± 3.2 kG. The negative sign corresponds to an average value at the south pole while the positive sign corresponds to an average value at the north pole.

In addition to the permanent magnets, it was desired to measure the magnetic fields of the three coils in order to validate Equation 3. The theoretical and experimental values obtained from all three cores for currents ranging from two to twenty amps, in increments of one amp, are listed in Table 3. Additionally, plots of theoretical values versus experimental values by core are shown in Figures 30 through 32.

Table 3. Theoretical and Experimental Magnetic Fields (Increasing Current, Constant Distance)

Current (A)	Magnetic Field (G)					
	Air Core		Iron Core		Steel Core	
	Theory	Actual	Theory	Actual	Theory	Actual
2	66.25	49.7	118.42	86.3	118.65	86
3	99.38	90.3	177.62	165	177.98	160
4	132.51	134	236.83	239	237.31	239
5	165.63	173	296.04	312	296.63	310
6	198.76	216	355.25	386	355.96	392
7	231.89	259	414.45	460	415.28	466
8	265.01	299	473.66	537	474.61	544
9	298.14	340	532.87	614	533.94	613
10	331.27	384	592.08	684	593.26	686
11	364.39	425	651.28	764	652.59	768
12	397.52	466	710.49	837	711.92	839
13	430.65	510	769.7	910	771.24	908
14	463.77	551	828.91	982	830.57	988
15	496.9	590	888.11	1055	889.89	1058
16	530.03	628	947.32	1128	949.22	1137
17	563.15	675	1006.53	1202	1008.55	1207
18	596.28	723	1065.74	1275	1067.87	1278
19	629.41	755	1124.94	1350	1127.2	1353
20	662.53	795	1184.15	1419	1186.53	1426

As discussed in Chapter III, Step 7, the relative permeability of a material can greatly vary depending on how the material was formed and treated. As such, it was necessary to determine the actual relative permeability of the iron and steel cores. This was accomplished by dividing the magnetic field of a core at each current by the corresponding magnetic field of the air core at the same current (see Equation 25) and taking the average of those values. The resultant relative permeabilities are as follows: iron core – 1.787304; steel core – 1.790887. These relative permeabilities were then used to calculate the theoretical values for the magnetic fields of the iron and steel cores.

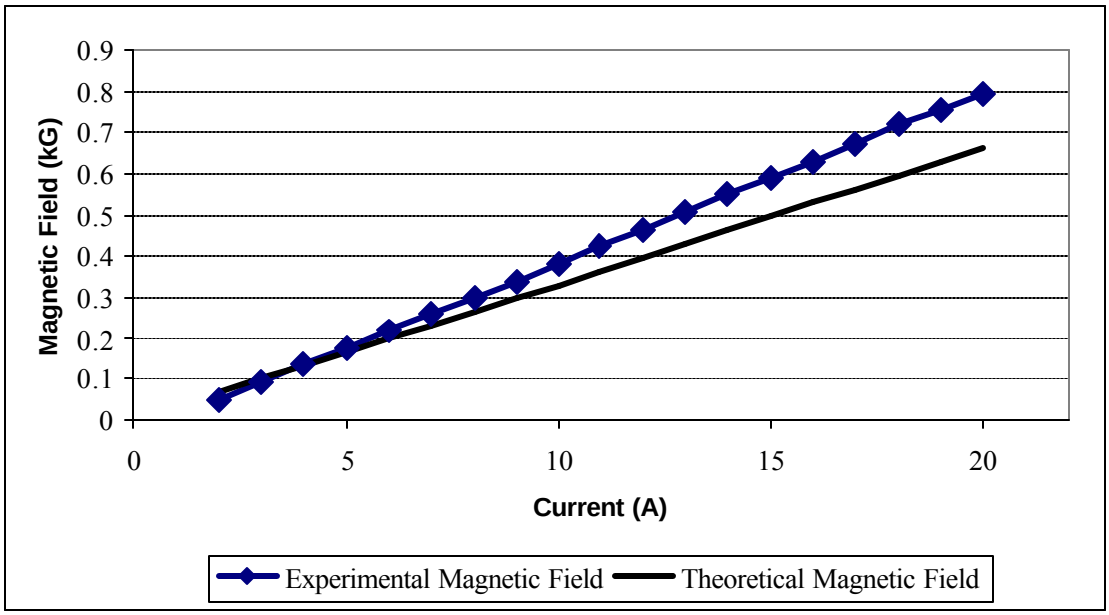

Figure 30. Magnetic Field vs. Current (Air Core)

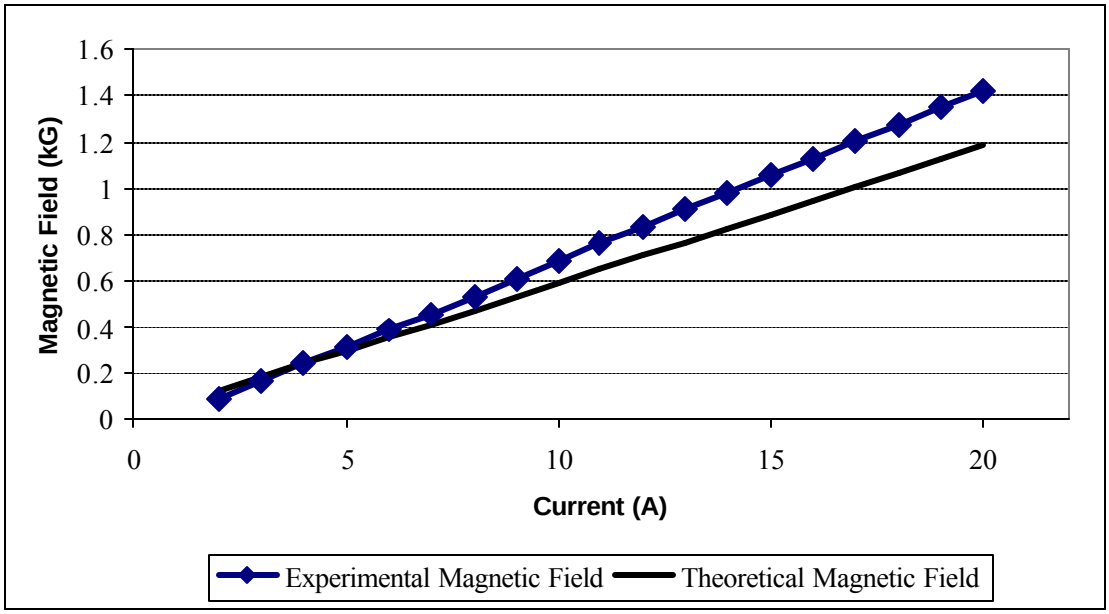

Figure 31. Magnetic Field vs. Current (Iron Core)

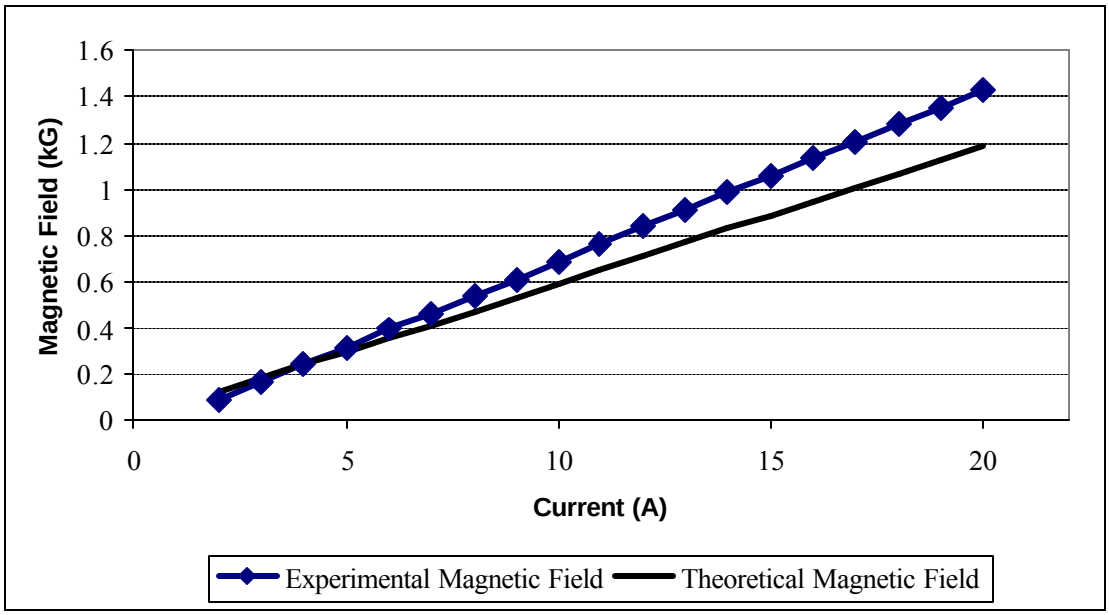

Figure 32. Magnetic Field vs. Current (Steel Core)

The current was limited to 20 amps so as not to significantly exceed the ampacity of the 14 gauge magnet wire used in the coil. As seen in Table 3 and Figures 30 through 32, Equation 3 underestimates the magnetic field by as much as 146 G for the air core (approximately 18%) and 260 G for the iron and steel cores (approximately 5%). While this shows the equation is not as accurate as hoped, it serves as a valid prediction tool for the TEFF. If the TEFF desires a certain magnetic field from a coil for a given current, they will be able to predict the minimum field produced by the coil at that current. For example, if they need a magnetic field of 464 G at a current of 8 A, they will be able to actually achieve a magnetic field of approximately 530 G when using the iron core. In order to get the desired 464 G, they will actually only need about 7 A of applied current.

An interesting phenomenon did occur regarding the uniformity of the magnetic field for the air core versus the iron and steel cores. With an air core coil, the assumption

is the magnetic field is fairly uniform within the core of the coil. This is especially true at the midpoint of the longitudinal axis where the magnetic field reaches a maximum (see Equation 3 and Figure 12, where $x_2 = -x_1$) [14, 21, 24]. At the opening of the core, the field is still fairly uniform. During the course of this experiment, the magnetic field was measured at varying distances still within the boundary of the core (see Figure 33). For the air core, the magnetic field varied less than 10% as measurements were taken from the longitudinal axis outward; however, with the iron and steel cores, the magnetic field doubled from the longitudinal axis to the boundary of the core with the aluminum spindle. This can be attributed to two things: the proximity of the edge of the core versus the center of the core to the coil's windings; and the size of the core. From the Biot-Savart law [14], the magnetic field of an individual wire is inversely proportional to the squared distance away from the wire. Because the diameter of the iron or steel core is

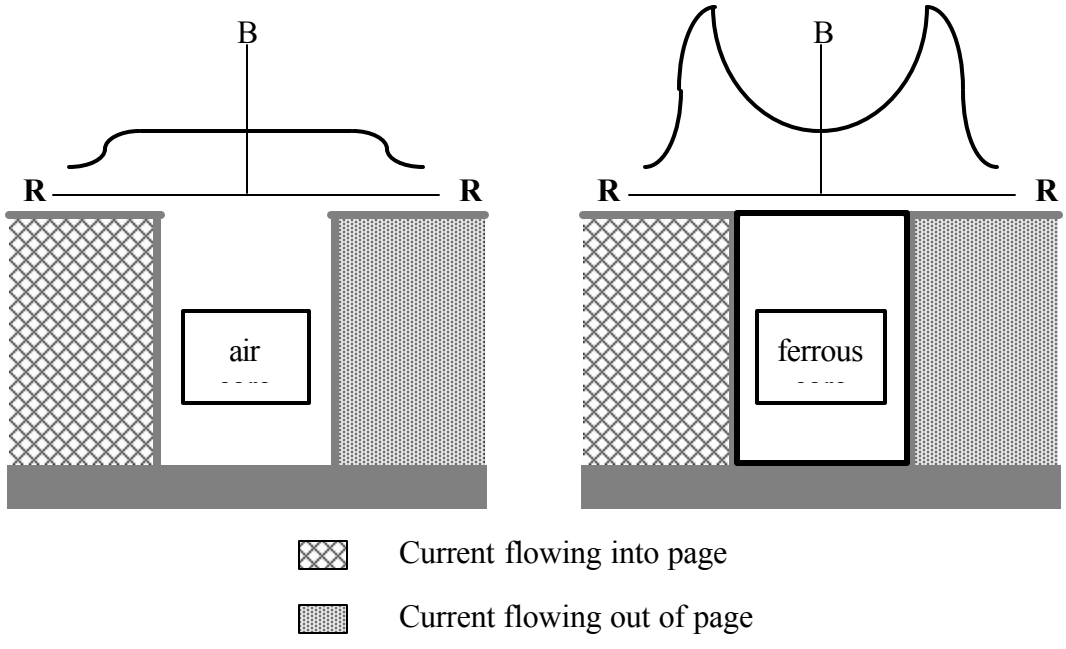

Figure 33. Magnetic Field at Increasing Radial Distance from the Longitudinal Axis

comparable to the diameter of the aluminum spindle (see Appendix E), the center of the core is far enough away from the nearest wire to permeate magnetic fields which are approximately half as strong as the magnetic fields at the core/spindle boundary. As such, the enhancement of the magnetic field along the longitudinal axis is much less than the enhancement at the boundary. This possibly occurred as a result of the field weakening as distance from the coil's wires increases; the field at the center of the core is not strong enough to line up as many magnetic domains as the field at the core/spindle boundary (see Figure 10). Fortunately, in the near vicinity of the longitudinal axis, the field remained uniform to the point of not significantly impacting the moment exerted on the beam as it vibrates.

Measure Magnetic Field of Cores with Increasing Distance at Constant Current.

One of the other highly desired outcomes of this experiment was to map the dependence of magnetic field on distance from the source. This is desired to give the TEFF the capability to determine where the magnetic field produced by the coil, and subsequently the torque exerted on the beam, becomes invaluable. As distance from the coil increases, the magnetic field weakens as shown in Figure 24. In addition to validating Equation 3 for increasing current, it was desired to validate Equation 3 at increasing distances.

Measurements of the axial field were taken from 0 to 5 cm in increments of 0.2 cm. The results are displayed in Table 4; the values in Table 4 are plotted graphically in Figures 34-36.

The theoretical and experimental values for the air core are very consistent, almost a one for one comparison throughout the entire length of the curve; however,

these results must be taken in context with Figure 30. As seen in Figure 30, the theoretical and experimental magnetic fields match well at currents roughly less than 8 A; so the randomly chosen current of 5 A actually contributes to the good comparison for the air core. It could be postulated the comparison would not go as well if the current was anywhere above 8 A.

Table 4. Theoretical and Experimental Magnetic Fields (Constant Current, Increasing Distance)

Distance (mm)	Magnetic Field (G)					
	Air Core		Air Core		Steel Core	
	Theory	Actual	Theory	Actual	Theory	Actual
0	189.6	174	338.8	320	339.5	320
2	176.2	173	315	370	315.6	367
4	163.3	162	291.9	368	292.4	360
6	150.8	149	269.6	353	270.1	344
8	139	139	248.4	335	248.9	322
10	127.8	127	228.4	316	228.9	300
12	117.3	116	209.7	295	210.1	278
14	107.6	107	192.2	263	192.6	255
16	98.5	99	176.1	242	176.4	234
18	90.1	92	161.1	220	161.4	212
20	82.4	84	147.3	201	147.6	195
22	75.3	77	134.7	182	134.9	178
24	68.9	71	123.1	169	123.3	162
26	62.9	65	112.4	151	112.7	149
28	57.5	61	102.7	138	102.9	135
30	52.5	56	93.8	127	94	124
32	47.9	51	85.7	120	85.9	112
34	43.8	48	78.3	112	78.4	105
36	40	45	71.5	105	71.6	96
38	36.5	41	65.3	95	65.4	88
40	33.3	38	59.6	90	59.7	81
42	30.4	34	54.4	84	54.5	72
44	27.8	31	49.6	77	49.7	64
46	25.3	28	45.3	72	45.4	61
48	23.1	26	41.3	67	41.4	56
50	21.1	24	37.6	62	37.7	52

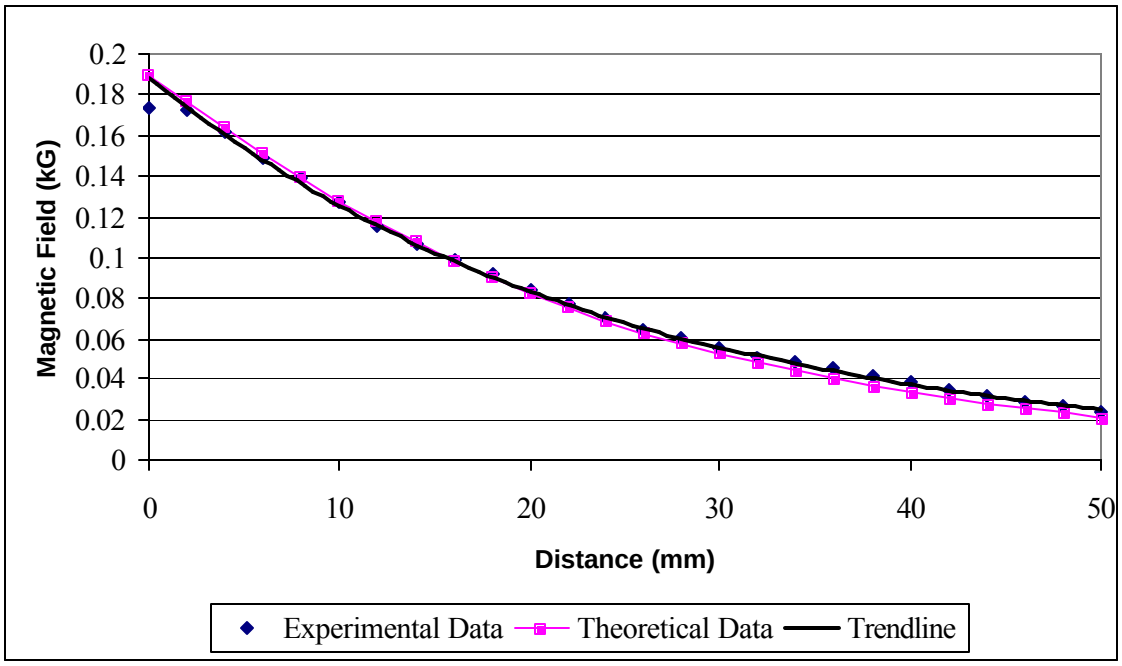

Figure 34. Magnetic Field vs. Distance (Air Core)

Just as there were inconsistencies with the theoretical models regarding the uniformity of the magnetic field with the ferromagnetic cores, there were also unexpected results when the current was held at 5 A and the distance was increased (see Figures 35 and 36). Theoretically, the maximum field should occur at the exposed surface of the ferromagnetic core; however, during the experiment, the maximum field was measured at a distance of 2 mm. The other interesting result was the field was more uniform at this distance than at the surface of the core. Readings were taken with the gaussmeter over the boundary of the core at a distance of 2 mm, and the results were a very uniform field throughout this region.

This outcome, though surprising, is actually beneficial for TEFF applications. There can be space between the beam, and its magnets, and the core, thereby preventing

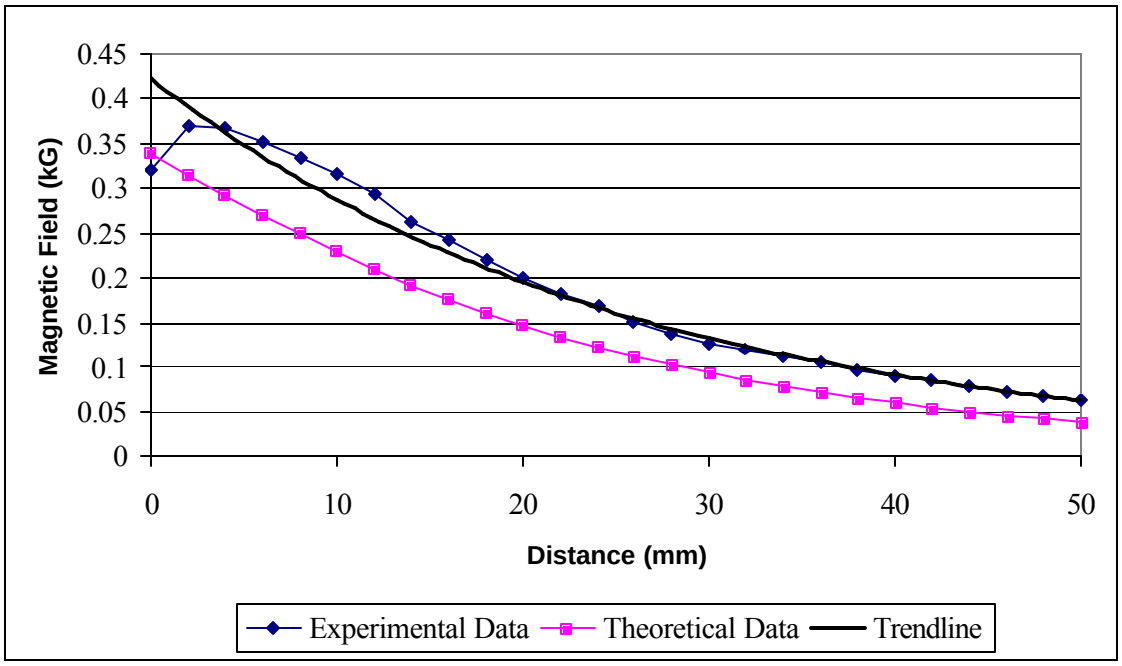

Figure 35. Magnetic Field vs. Distance (Iron Core)

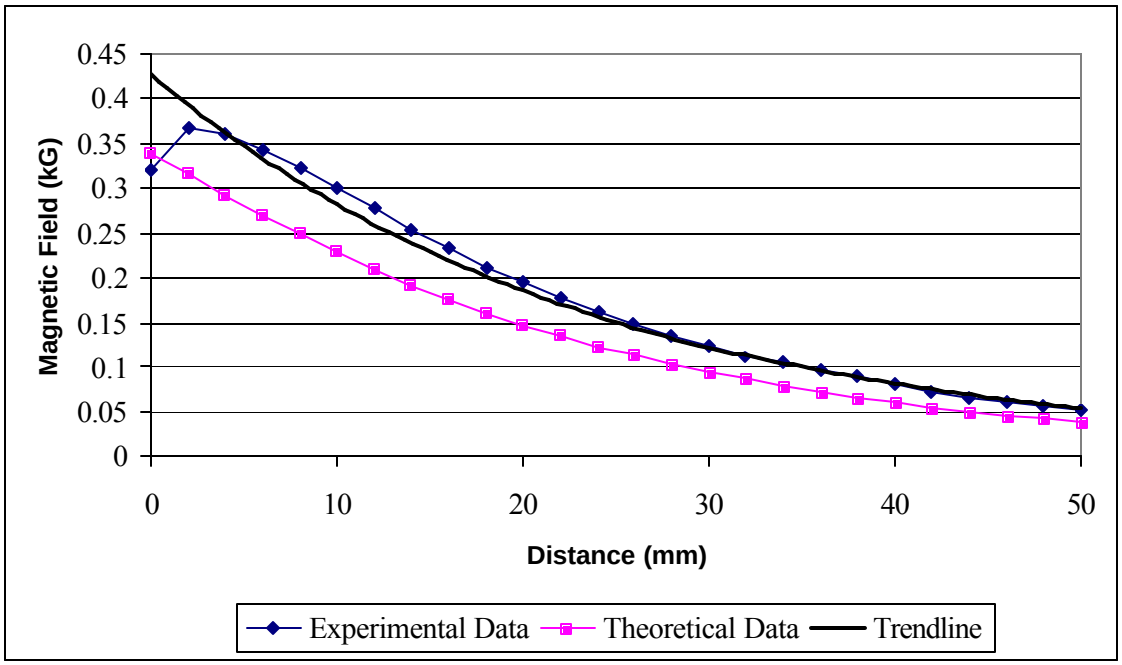

Figure 36. Magnetic Field vs. Distance (Steel Core)

any possible physical interaction between the beam and the surface of the core. Additionally, the theoretical model of the magnetic dipole of the magnets is more accurate as distance increases between the magnets and the source of the external magnetic field, in this case the coil (see Chapter II, Modeling Permanent Magnets as Magnetic Dipoles).

There are two possible reasons for these phenomena; both as a result of core material extending beyond the upper boundary of the coil's windings. The windings occupy a height on the aluminum spindle of 4.98 cm; the cores have a height of 5.4 cm (see Appendix F for core and spindle dimensions). This leaves a 0.42 cm piece of core receiving a differently oriented magnetic field than the other 4.98 cm of core material. First, concerning the maximum field at a distance, the magnetic field vector at the center of the core may not be perpendicular to the core's surface (parallel to its longitudinal axis). Because the probe only measures fields perpendicular to its active area (see Figure 27), the probe is only detecting the perpendicular component of magnetic field at the core's surface. At a further distance, in this case 2 mm, the magnetic field vector is more parallel to the core's axis and therefore has a larger perpendicular component impacting the probe. Second, pertaining to the uniformity at a distance, the magnetic field vector has a larger magnitude due to the proximity of the wires, but the field lines in this region do not remain parallel to the longitudinal axis as long as those at the center of the core. Referencing Figures 8, 9, and 11, the magnetic field lines in this region diverge quickly compared to those along the core's axis. Therefore, at further distances, the magnetic field lines intersecting the probe actually originate somewhere between the core's axis and its edge (see Figure 37).

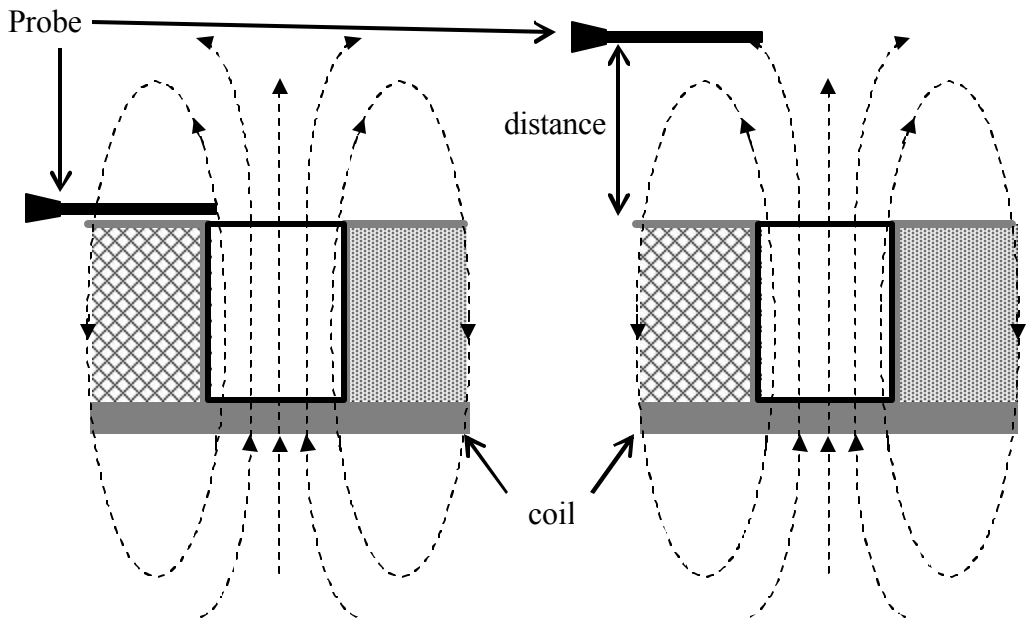

Figure 37. Distance Affects Intersecting Magnetic Field Lines at Core's Edge

Measure Experimental Torque with Increasing Current.

Knowing all magnetic fields makes it possible to calculate the magnetic dipole moment of the permanent magnets and the theoretical torque exerted on them.

The magnetic dipole moment for the permanent magnets was calculated using the average magnetic field value of 0.32 T discussed previously in this chapter (see Measure Magnetic Fields of All Magnets). As such, the magnetic dipole moment was calculated using Equation 6 to be 0.061451 A-m^2. With the $0.8\overline{3}$ scaling factor as discussed in Chapter II (see Modeling Permanent Magnets as Magnetic Dipoles), the magnetic dipole moment becomes 0.051209 A-m^2.

The theoretical torque was calculated using experimentally measured magnetic fields. The experimental torque was then measured as shown in Figure 28. Before each core was used, the mass on the scale was recorded and subsequently subtracted from all

force measurements. The theoretical and experimental results are listed in Table 5. Graphical comparisons are shown in Figures 38 through 40.

Table 5. Theoretical and Experimental Torques (Increasing Current, Constant Distance)

Current (A)	Torque (N-m)					
	Air Core		Air Core		Steel Core	
	Theory	Actual	Theory	Actual	Theory	Actual
2	.002545	.001982	.004419	.002694	.004404	.002833
3	.004624	.004196	.00845	.006193	.008193	.006379
4	.006862	.006751	.012239	.009274	.012239	.009646
5	.008859	.008221	.015977	.012247	.015875	.012572
6	.011061	.010002	.019767	.015251	.020074	.015638
7	.013263	.012541	.023556	.01813	.023863	.019121
8	.015312	.014523	.027499	.021428	.027858	.022171
9	.017411	.016272	.031442	.024215	.031391	.025098
10	.019664	.018363	.035027	.027033	.035129	.028179
11	.021764	.020097	.039124	.029603	.039329	.031647
12	.023863	.022001	.042862	.032746	.042964	.034836
13	.026117	.023704	.0466	.035347	.046498	.037902
14	.028216	.025655	.050287	.037933	.050595	.040782
15	.030213	.027544	.054026	.040565	.054179	.040844
16	.032159	.029588	.057764	.042934	.058225	.043631
17	.034566	.031399	.061553	.044327	.061809	.046216
18	.037024	.033133	.065292	.047161	.065445	.048864
19	.038663	.035332	.069132	.050149	.069286	.05148
20	.040711	.036927	.072666	.053431	.073024	.05419

Referencing Figures 38 through 40, it is seen the comparison between the theoretical and experimental values for the air core is decent. The largest discrepancy occurs at 20 A and is less than 10%; however, the same comparison on the iron and steel cores is not as good. The largest discrepancy, for both cores, is approximately 24%. On all three cores, it can be seen the comparison is better at lower currents.

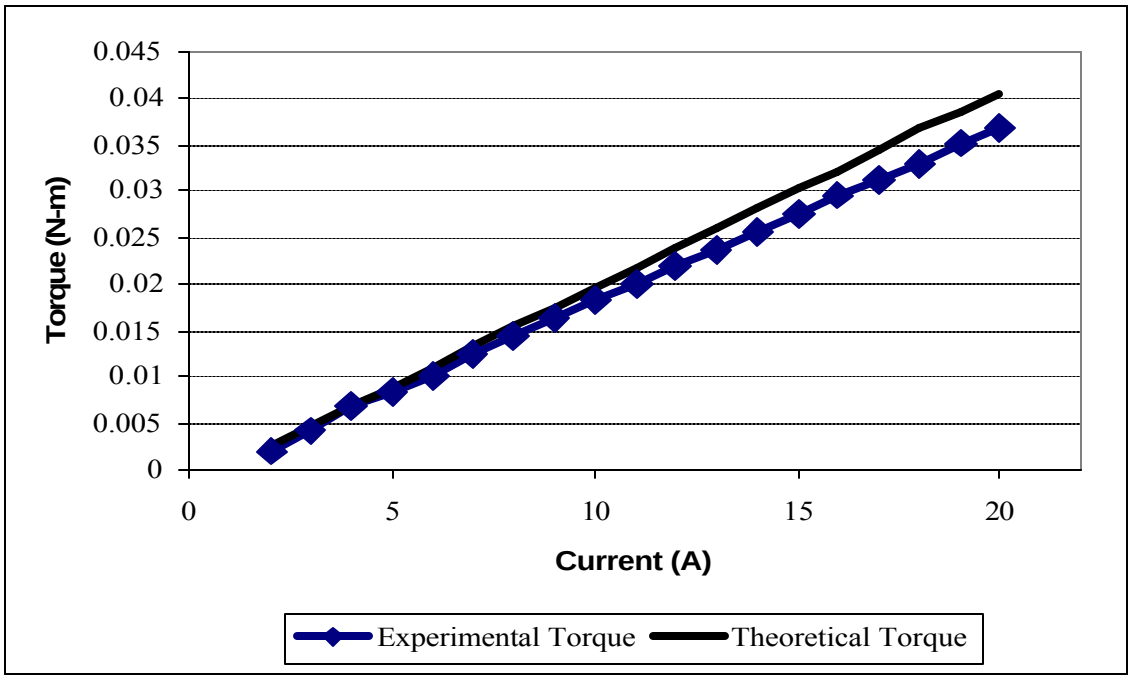

Figure 38. Torque vs. Current (Air Core)

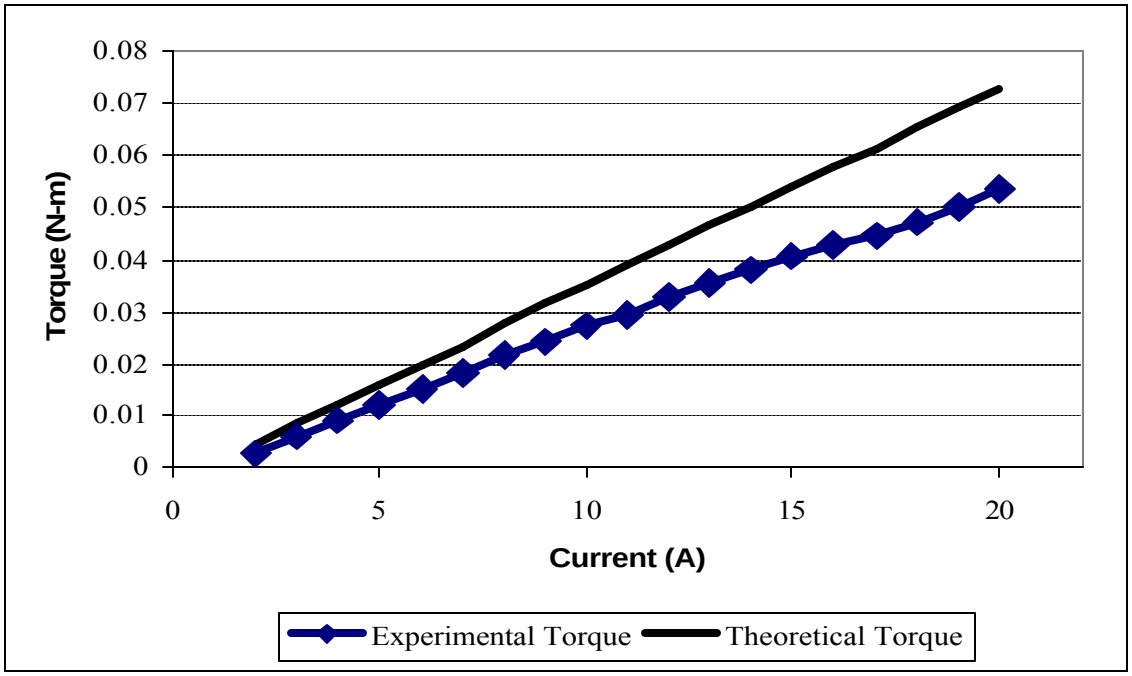

Figure 39. Torque vs. Current (Iron Core)

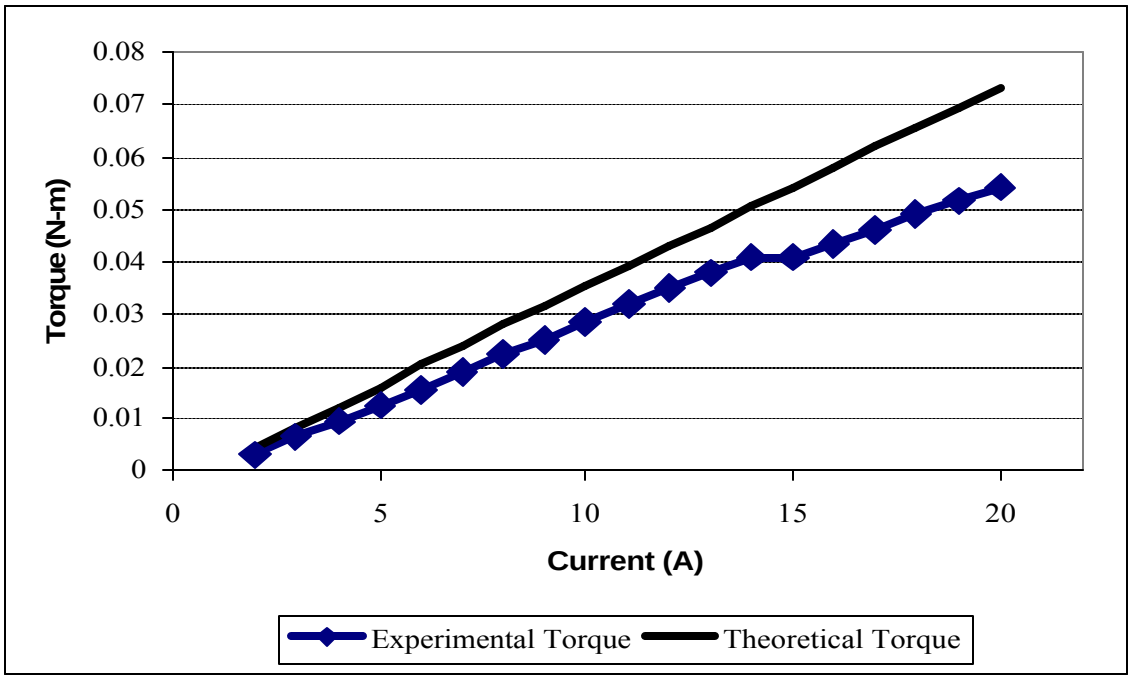

Figure 40. Torque vs. Current (Steel Core)

A possible reason is the existence of an attractive force between the coil, with a ferromagnetic core, and the permanent magnets. The model being used for the experiment deals only with the torque being applied to the permanent magnets. The assumption was made the attractive force would be significantly weaker than the torque; however, in a static configuration, like this experiment, the attractive force pulls the magnets toward the coil. The resultant effect is a loss of torque. As current increases, experimental measurements indicate the attractive force strengthens at a rate exceeding the rate at which the torque increases. Hence, the attractive force has more of an effect at higher currents as indicated in Figures 38-40. Furthermore, it has more of an effect with the ferromagnetic cores because the magnetic fields have a higher magnitude and thus a higher attractive force than the air core.

When conducting vibration experiments, the attractive/repulsive force would not be as much of a factor because the experiment is no longer static; the net force on the beam's magnets would effectively be zero. As the beam vibrates due to the torque, it vibrates so quickly the attractive/repulsive force has almost no effect when compared to the effect of the torque.

Observations made during the course of this research show the beam being lifted by the suspension wire (see Figure 2). This is consistent with pendulous motion; the suspension wire is flexible and vibrates at the same frequency as the beam. As it vibrates, it does not stay straight and pulls the beam to a higher position over the coil. At a given frequency, the wire will attain a modeshape much the same as the beam does, thereby keeping the beam at a quasi-constant distance from the coil. The changes in distance are so small the distance can be considered constant.

It was desired to use the actual magnetic fields as measured during the experiment to calculate the torque; however, a final comparison was made using the theoretical magnetic field, calculated using Equation 3, to calculate the theoretical torque. Interestingly, the experimentally measured moment compared better to this "totally theoretical" calculation than it did to the torque calculation using the experimentally measured magnetic field values (see Figures 41-44). This is extremely beneficial for the TEFF. Using Equations 3, 4, and 16, they will be able to achieve a torque which is no more than $\pm 10\%$ for any of the cores from the predicted torque for a given current.

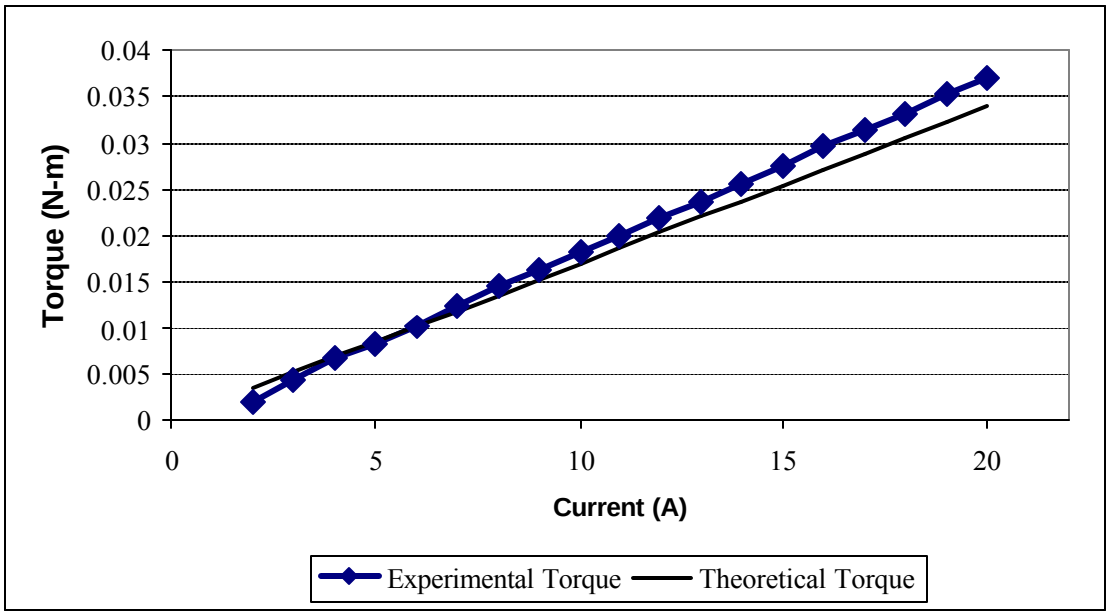

Figure 41. Comparison of Torques Using Theoretical Magnetic Field (Air Core)

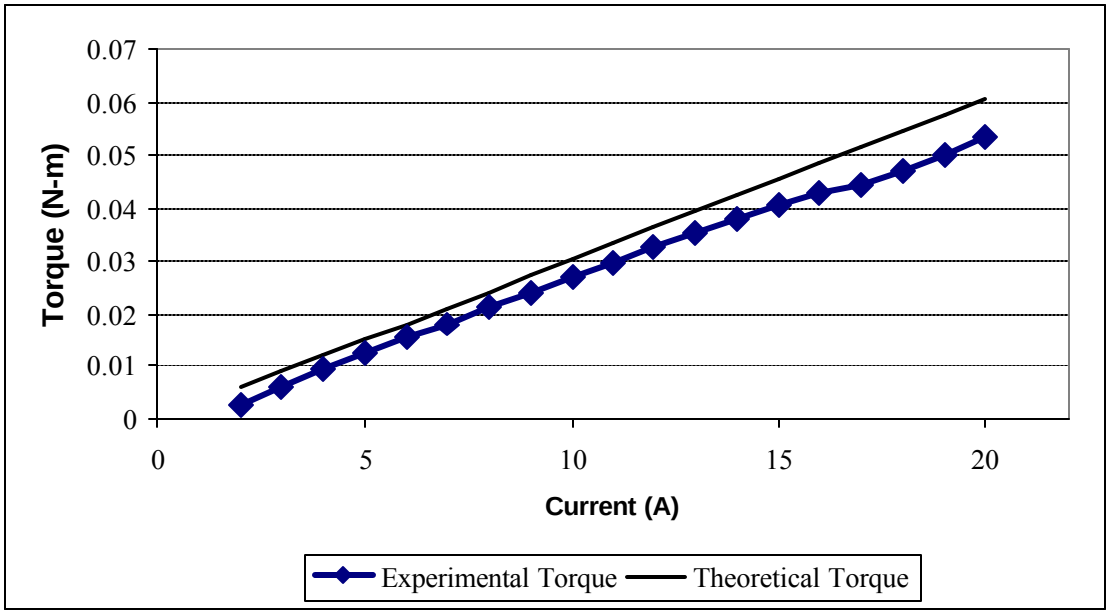

Figure 42. Comparison of Torques Using Theoretical Magnetic Field (Iron Core)

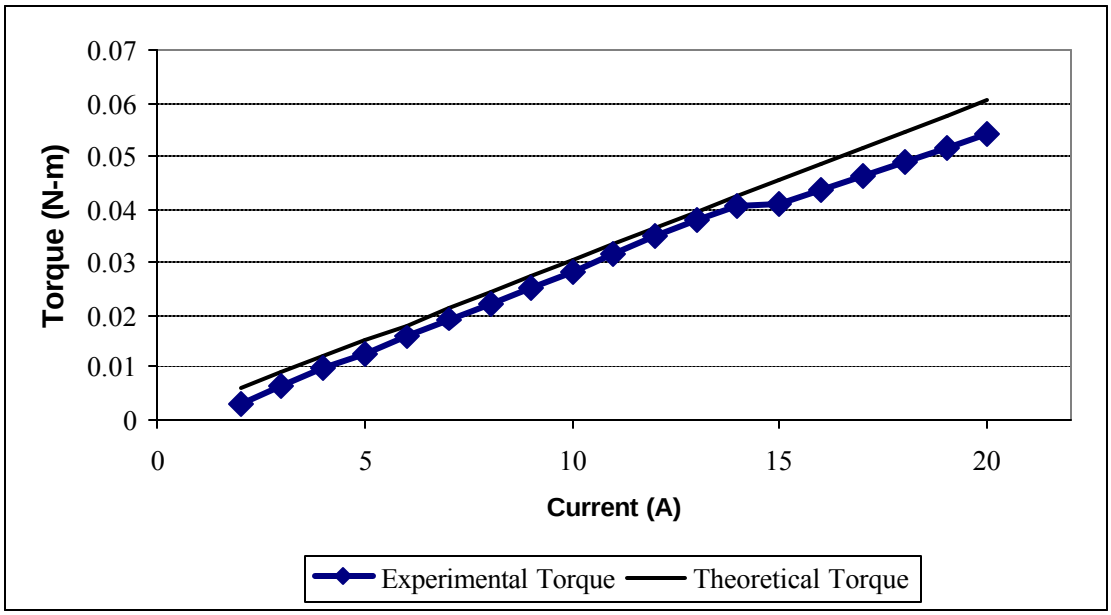

Figure 43. Comparison of Torques Using Theoretical Magnetic Field (Steel Core)

Measure Experimental Torque with Increasing Distance.

The torque was measured under increasing distance conditions, similar to those of the magnetic field measurements, and compared to a theoretical torque calculated at increasing distances. The theoretical torque was calculated without a scaling factor to see how the experimental torque behaved; theoretically, as distance increases, the scaling factor should approach 1. The torque was calculated using actual and theoretical magnetic field values, and the results are displayed in Figures 44 through 46.

When analyzing the results of the air core as shown in Figure 44, all three curves compare very nicely. This can be attributed to the fact the magnetic field measurements for the air core were taken a further distance from the source of the magnetic field, the

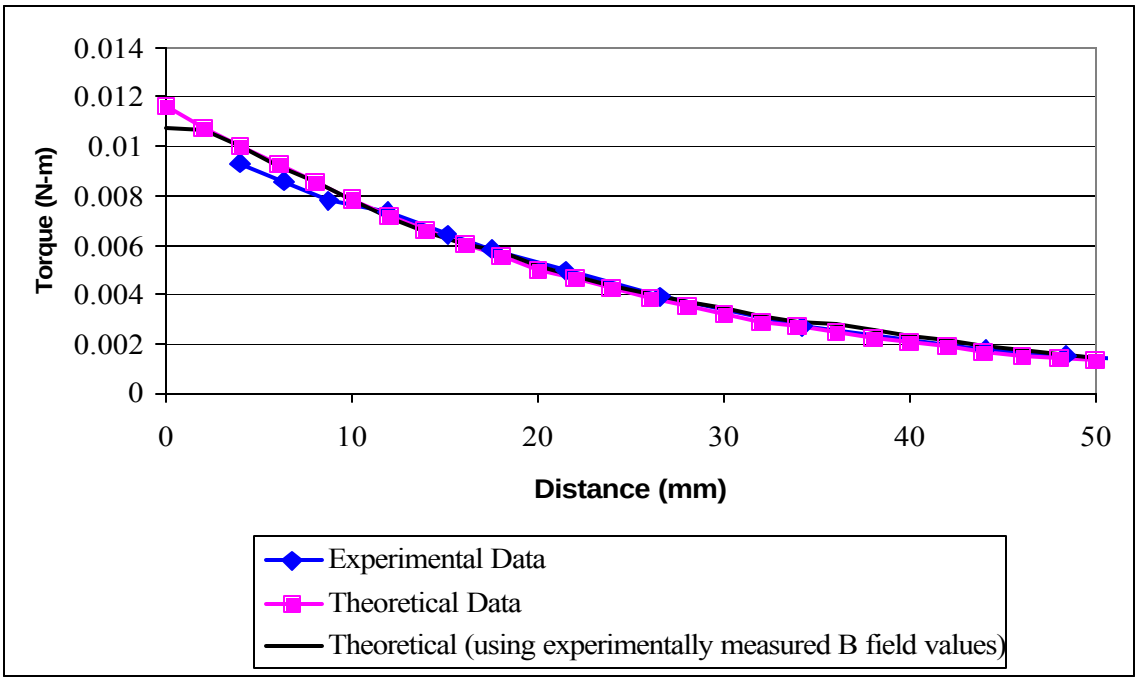

Figure 44. Torque vs. Distance (Air Core)

coil's wires, than the source of the magnetic field with a ferromagnetic core, the core itself. As mentioned earlier in Chapter II, the accuracy of the torque calculation (Equation 4) is dependent on the magnets being at least 5 times their largest dimension from the source of the external magnetic field. The largest dimension of the permanent magnets is their combined length with the beam spacer of 7.62 mm (see Figure 16). The first measurement was taken 3.97 mm from the spindle's surface. Geometry yields 29.45 mm ($d = \sqrt{(3.97 + 3.175)^2 + 28.575^2}$, where 3.175 = spindle thickness, 28.575 = radial distance to the nearest wire). 5 times the largest dimension of the magnets is 38.1 mm. Therefore, Equation 4 is more accurate when compared to air core measurements than measurements taken with the iron and steel cores. In Figure 44, all three curves align at further distances, indicating the scaling factor does approach 1.

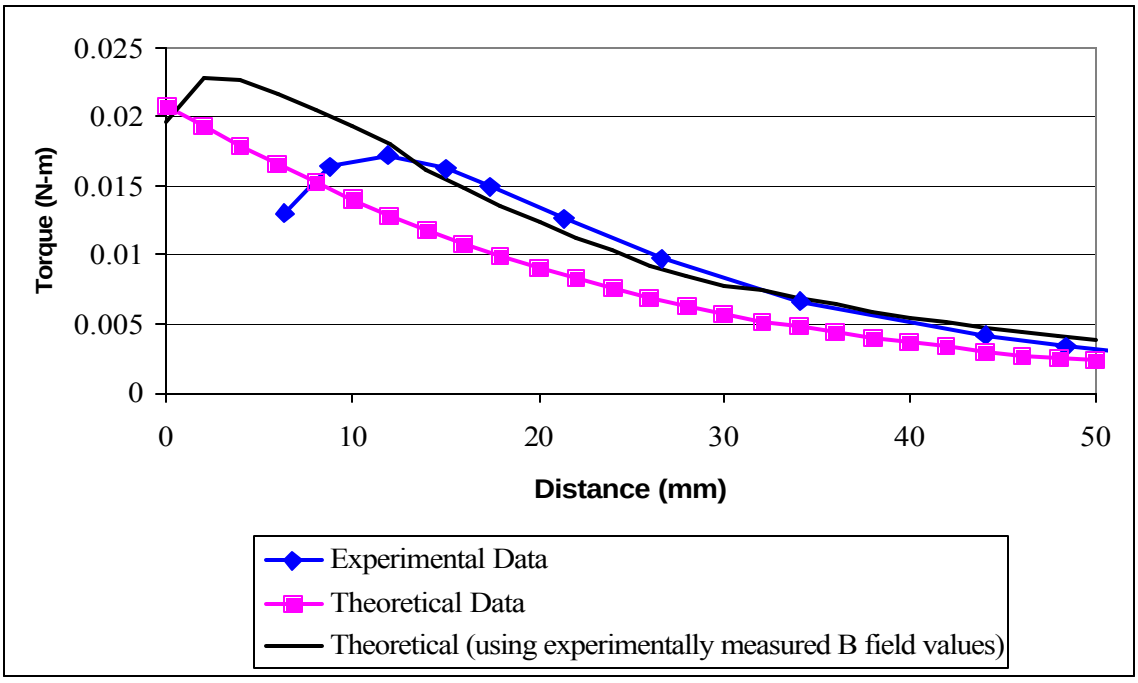

Figure 45. Torque vs. Distance (Iron Core)

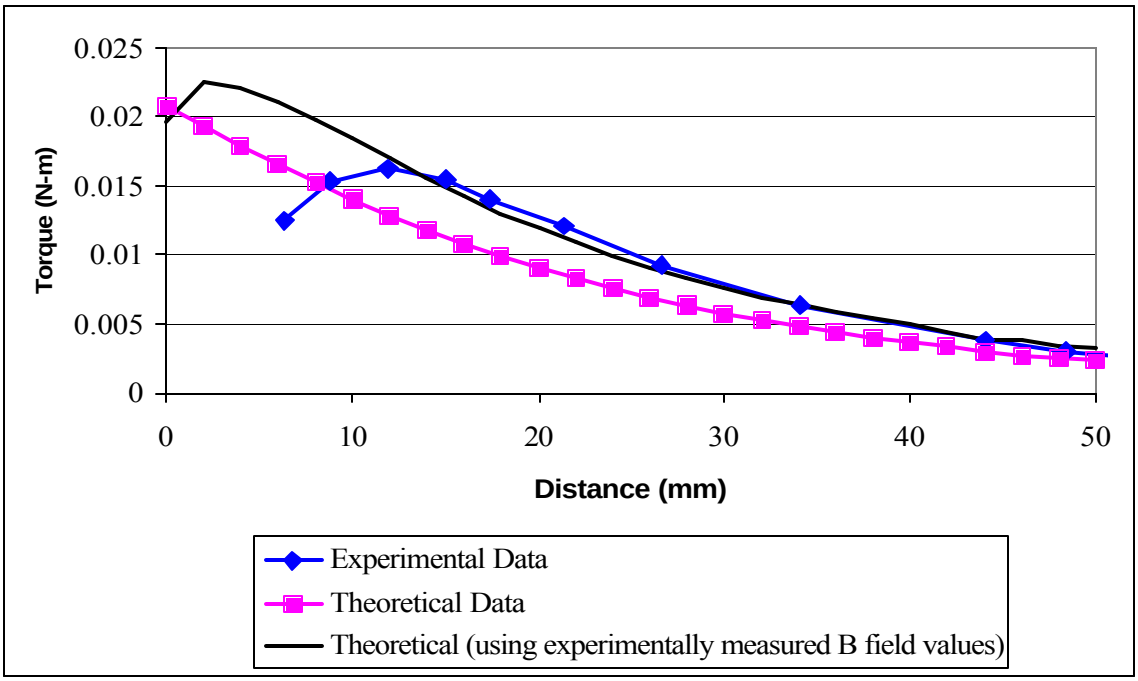

Figure 46. Torque vs. Distance (Steel Core)

Focusing now on the ferromagnetic cores, the phenomenon observed with the magnetic field where the maximum field was not measured at the core's surface was observed with the torque measurements as well; however, in Figures 45 and 46, the maximum moment reading occurred at a further distance than the maximum field measurement. This distance possibly corresponds to a distance where the attractive magnetic force approaches zero. Unlike the air core, the actual torque is higher than the theoretical torque, so a scaling factor greater than 1 at distances between 10 mm and 40 mm would be necessary when using Equation 4 to predict the torque at a distance. Finally, it can be see in Figures 45 and 46, similar to Figure 44, the scaling factor does approach 1 as the distance is increased; however, the torque values at these distances (greater than 40 mm) are so small they may not be of value for damping and fatigue analysis (these torques will not produce vibrations with displacements as large as those produced by torques at closer distances, where the distance is approximately 10 mm).

TEFF Applications

The intent of this thesis was to determine the accuracy of Equations 3, 4, and 6 so the TEFF would be able to use them to predict bending moments in vibrating beams. As discussed previously in this chapter, this intent has been met, but that doesn't answer the question, "How can they be used for TEFF applications?"

With this in mind, there are three ways the TEFF can use the results of this thesis effectively. First, they can reference any of the graphical figures in this section (Figures 30-32, 34-36, and 38-46) to approximately determine a magnetic field and torque for a given current or distance. Second, they can reference the following table (Table 6) for a

desired moment and choose the coil size which will give them this moment for a given current. Finally, they can use the Mathcad^{TM} spreadsheets in Appendices C and D.

Before using this table, several issues must be addressed:

1. Because Equation 3 is so complex, some of the variables had to be held constant. The variables held constant for Table 6 are x_1, x_2, and I (see Figure 12). x_1 and x_2 were held constant due to their correspondence with the height of the TEFF's existing coil; the TEFF's current coil height worked very well for establishing a uniform magnetic field in the core of the coil. However, if a new coil is built with a height of 5.08 cm (2 in) and the beam is suspended over the coil at a distance of 1 mm, then x_1 will equal 4.175 mm and x_2 will equal 5.4975 cm. The current, I, was set at 5 Amps; because I is outside the natural log portion of the equation, it is a simple mathematical calculation to convert the values in Table 6 for a 5 Amp current to values for any other current. For example, if the TEFF wanted to predict a bending moment at *M* Amps, simply multiply the values in Table 6 by *M*/5 (where *M* equals the DC or AC_{rms} value of current applied to the coil).

2. Values from Equation 3 were calculated with increasing values for R_1 and R_2; however, as R_1 and R_2 increase, the number of windings of wire also increases, which leads to the second parameter that must be held constant—the wire gauge. For Table 6, the wire gauge was set at 14 AWG; 14 gauge magnet wire has an approximate diameter of 1.867319535 mm (0.073516517 in). Knowing the diameter makes it possible to estimate the turns per meter, n from Equation 3, as follows:

1. The reciprocal of the wire diameter, in meters, gives the wires/meter

2. For a given R_1, if R_2 increases by integer increments of the wire's diameter, m, where m = 1, 2. . . .16 for Table 6, the turns/meter, n, is equal to m divided by the wire diameter in meters (m/0.001867319535), see Table 7.

3. The values in Table 6 are for a solenoid (no ferromagnetic core inserted). If a ferromagnetic core is inserted, the relative permeability will have to be determined as described in Step 7 of the experimental plan (see Chapter III).

With these constraints in mind, Table 6 can effectively be used to predict bending moments at any current for a coil with a height of 5.08 cm (2 in) at the inner and outer radius chosen from Table 6.

Table 6. Bending Moments for a 5.08 cm Tall Coil with a 5 Amp Current (DC or AC_{rms})

R_1 (cm)	R_2 (cm)	Bending Moment (N-m × 10^{-6})	R_1 (cm)	R_2 (cm)	Bending Moment (N-m × 10^{-6})	R_1 (cm)	R_2 (cm)	Bending Moment (N-m × 10^{-6})
0.25	0.4367	1.4289	0.5	0.6867	2.6502	0.75	0.9367	3.4543
	0.6235	3.8109		0.8735	5.9348		1.1235	7.3077
	0.8102	3.9046		1.0602	9.6680		1.3102	11.446
	0.9969	10.503		1.2469	13.720		1.4969	15.788
	1.1837	14.459		1.4337	18.000		1.6837	20.275
	1.3704	18.670		1.6204	22.444		1.8704	24.866
	1.5571	23.064		1.8071	27.004		2.0571	29.527
	1.7439	27.589		1.9939	31.644		2.2439	34.232
	1.9306	32.206		2.1806	36.337		2.4306	38.961
	2.1173	36.883		2.3673	41.059		2.6173	43.697
	2.3041	41.598		2.5541	45.795		2.8041	48.428
	2.4908	46.331		2.7408	50.529		2.9908	53.141
	2.6775	51.067		2.9275	55.249		3.1775	57.830
	2.8642	55.793		3.1142	59.947		3.3642	62.485
	3.0510	60.500		3.3010	64.614		3.5510	67.101
	3.2377	65.178		3.4877	69.244		3.7377	71.373

Table 6. Bending Moments for a 5.08 cm Tall Coil with a 5 Amp Current (DC or AC_{rms}) (cont)

R_1 (cm)	R_2 (cm)	Bending Moment (N-m × 10^{-6})	R_1 (cm)	R_2 (cm)	Bending Moment (N-m × 10^{-6})	R_1 (cm)	R_2 (cm)	Bending Moment (N-m × 10^{-6})
1	1.1867	3.9606	1.25	1.4367	4.2834	1.5	1.6867	4.4899
	1.3735	8.1754		1.6235	8.7296		1.8735	9.0821
	1.5602	12.572		1.8102	13.291		2.0602	13.744
	1.7469	17.099		1.9969	17.932		2.2469	18.449
	1.9337	21.717		2.1837	22.626		2.4337	23.178
	2.1204	26.395		2.3704	27.349		2.6204	27.915
	2.3071	31.110		2.5571	32.084		2.8071	32.645
	2.4939	35.844		2.7439	36.818		2.9939	37.358
	2.6806	40.579		2.9306	41.538		3.1806	42.046
	2.8673	45.305		3.1173	46.236		3.3673	46.701
	3.0541	50.011		3.3041	50.902		3.5541	51.316
	3.2408	54.689		3.4908	55.531		3.7408	55.888
	3.4275	59.332		3.6775	30.118		3.9275	60.411
	3.6142	63.933		3.8642	64.658		4.1142	64.882
	3.8010	68.490		4.0510	69.147		4.3010	69.300
	3.9877	72.996		4.2377	73.584		4.4877	73.662
R_1 (cm)	R_2 (cm)	Bending Moment (N-m × 10^{-6})	R_1 (cm)	R_2 (cm)	Bending Moment (N-m × 10^{-6})	R_1 (cm)	R_2 (cm)	Bending Moment (N-m × 10^{-6})
1.75	1.9367	4.6189	2	2.1867	4.6938	2.25	2.4367	4.7293
	2.1235	9.2980		2.3735	9.4172		2.6235	9.4657
	2.3102	14.013		2.5602	14.153		2.8102	14.196
	2.4969	18.747		2.7469	18.886		2.9969	18.909
	2.6837	23.482		2.9337	23.606		3.1837	23.596
	2.8704	28.208		3.1204	28.303		3.3704	28.250
	3.0571	32.914		3.3071	32.969		3.5571	32.865
	3.2439	37.591		3.4939	37.598		3.7439	37.436
	3.4306	42.233		3.6806	42.184		3.9306	41.958
	3.6173	46.834		3.8673	46.723		4.1173	46.429
	3.8041	51.389		4.0541	51.212		4.3041	50.845
	3.9908	55.895		4.2408	55.647		4.4908	55.206
	4.1775	60.349		4.4275	60.027		4.6775	59.509
	4.3642	64.748		4.6142	64.350		4.8642	63.754
	4.5510	69.090		4.8010	68.614		5.0510	67.938
	4.7377	73.374		4.9877	72.819		5.2377	72.063

Table 7. Turns Per Meter as Outer Radius Increases by Integer Increments of Wire Diameter

m	1	2	3	4	5	6	7	8
turns/meter (n)	536	1071	1607	2142	2678	3213	3749	4284
m	9	10	11	12	13	14	15	16
turns/meter (n)	4820	5355	5891	6426	6962	7497	8033	8568

An example of how to use Tables 6 and 7 follows:

1. Choose an inner and outer radius for the proposed coil. Let R_1 = 1.75 cm and R_2 = 3.8041 cm.
2. R_2 - R_1 = 2.0541 cm. 2.0541 cm $\div$ 0.1867319535 cm (wire diameter) = 11.
3. In Table 7, when m = 11, there are approximately 1607 turns/m on the proposed coil.
4. In Table 6, with R_1 = 1.75 cm and R_2 = 3.8041 cm, the possible bending moment is 51.389×10^{-6} N-m with 5 Amps of current applied to the coil.
5. For the possible bending moment at 14 Amps. Multiply the value at 5 Amps from Table 6, 51.389×10^{-6} N-m, by 14/5. This gives a possible bending moment at 14 Amps of 143.8892×10^{-6} N-m.

One of the limits of Table 6 is it doesn't provide moment values at a distance above the coil. Which leads to the final option for the TEFF: using the Mathcad™ spreadsheets in Appendices C and D. By using these spreadsheets, TEFF personnel can vary any parameters and obtain predictive results for magnetic field and torque at any distance above the coil.

V. Conclusions

The conclusions presented in this chapter are based on results discussed in Chapter IV. No new results will be presented in this chapter.

The assumption was made the titanium beam, as a spacer between the two rare earth magnets (see Figure 16), would not impact the magnetic field and the magnetic dipole moment of the magnets (the beam increased the length used to calculate the volume of the magnets which was in turn used to calculate the magnetic dipole moment of the magnets). **Conclusion**: Results from the experiment indicate this assumption held true. **Conclusion:** The magnetic dipole model of the permanent magnets attached to the beam is an accurate model.

Conclusion: Based on observations and results discussed in Chapter IV, the equations for the magnetic field of a finite solenoid (Equation 3), the magnetic dipole moment of a permanent magnet (Equation 6), and the torque exerted on the magnets (Equation 4) can be used to predict torque from an electromagnetic coil. **Recommendation:** When predicting torque, use calculated values of the coil's magnetic field from Equation 3, not actual values measured experimentally.

The coil used for this research does not have an optimal configuration. Several concepts need to be addressed.

Conclusion: The 14 gauge magnet wire limits the possible magnetic field by limiting the turns/meter. **Recommendation:** A new coil could use 16 or 18 gauge wire

which would increase the number of windings on the spindle and therefore increase the magnetic field.

Conclusion: The inner and outer radii of the aluminum spindle are too large; as a result, the relative permeability of each ferromagnetic core may be higher than the value calculated and reported in Chapter IV. **Recommendation:** Smaller radii would decrease the distance to the longitudinal axis of the coil and therefore intensify the magnetic field. With a smaller coil, a smaller diameter core could be inserted. From Chapter IV, the strongest magnetic field was observed at the spindle/core interface. If the coil was smaller, those magnetic field lines would be condensed into a smaller area and intensify the overall magnetic field.

Conclusion: The wires were wrapped on the aluminum spindle; the thickness of the spindle created an unnecessary gap between the wires and the ferromagnetic cores. **Recommendation:** A new coil could be wound with no space between the wires and the core to ensure the strongest magnetic field induced by the wire would go directly into the core, not the aluminum spindle. Ideally, the wires should be wound directly onto the core.

Conclusion: Finally, the coil has no cooling system. Much time was lost waiting for the coil to cool after collecting measurements; if the coil had a cooling system, not only would this time not be lost, but the coil could operate longer without the risk of overheating and potentially melting the copper wire. **Recommendation:** Design and incorporate a simple cooling system.

Conclusion: The existing coil's windings were 4.98 cm in height while the metallic cores had a height of 5.4 cm. **Recommendation:** The core height should be the

same as the height of the windings to ensure once again the strongest magnetic field can be used to vibrate the beam. Furthermore, if the core height matched the winding height, the maximum magnetic field could potentially agree with the theoretical model and be observed at the core's surface as predicted by Equation 3.

The assumption was made the magnetic field would decrease with increasing distance from the coil; it was experimentally observed the magnetic field increased until a 2 mm distance was reached when it began to decrease. **Conclusion:** The assumption proved true at distances greater than 2 mm. **Recommendation:** The core height and the height of the windings should be equal.

Assumed field would be uniform over the surface of the core; the field was not uniform, especially with the ferromagnetic cores. **Conclusion:** The assumption was not validated. **Recommendation:** The core height and the height of the windings should equal, and a smaller inner radius for the coil should be used. As a result, the ferromagnetic core will have a smaller diameter as well.

Conclusion: The coil heats due to resistance heating. This resistance heating might detract from the actual current flowing through the coil. For this experiment, the ammeter displayed how much current was being applied to the coil. **Recommendation:** Use an ammeter to measure current exiting the coil; any ohmic losses could be extrapolated and could be compensated for in the theoretical models. **Recommendation:** Develop a simple cooling system to keep the coil cool and counteract resistance heating.

Conclusion: The attractive force between the coil and the rare earth magnets potentially counteracted the torque. **Recommendation:** An alternative setup could be used to measure the magnitude of the attractive force in order to determine its impact on

the torque. This type of setup could provide better insight into the complex force and torque interaction between the two magnetic fields. Results from another experiment could provide an accurate model of the force detracting from the torque.

Conclusion: As distance from the coil increased, the scaling factor used for the magnetic dipole moment calculation (Equation 16) did approach one; however, at distances between 10 and 20 mm, the maximum moment was observed for the iron and steel cores. As mentioned in Chapter IV, at these distances, the scaling factor proved to be greater than one; therefore, even though the scaling factor approaches one at further distances (beyond 40 mm), the electromagnetic torque is so small it cannot induce displacements large enough to induce fatigue. **Recommendation:** To fatigue the specimen with the existing coil, the torque values obtained between 10 and 20 mm should be used. **Recommendation:** Build a new coil where the coil height and the core height are equal; this could potentially move the point of maximum torque closer to the coil and core.

Conclusion: Large discrepancies were observed between experimental and theoretical results. **Recommendation:** Better quality control on a new coil could reduce "imperfect windings." The equations are developed based on a perfectly symmetric coil; in reality, the windings are not spaced evenly, thus an imperfect coil. Using a smaller gauge wire could limit the impact of "imperfect windings" as well. **Recommendation:** Build a new coil where the height of the coil and the height of the core are equal. **Recommendation:** Measure current exiting coil; if less current is exiting the coil than entering, the magnitude of the magnetic field would not be uniform through the length of the wire.

Appendix A: Glossary of Terms and Definitions

AC: Alternating Current; electric current that reverses direction in a circuit at regular intervals [27].

AFRL: Air Force Research Laboratory, Wright-Patterson Air Force Base, OH.

Area Vector: a vector whose direction is normal to the plane of the current loop (in the sense of the right hand rule relative to the direction of the current) and whose magnitude equals the area of the loop [25:9].

DC: Direct Current; electric current flowing in one direction [27].

FEM: Finite Element Method; the elastic continuum (with its infinite degree of freedom) is modeled by a finite number of structural elements of finite size, interconnected only at their nodal points; forces between the elements can only be transferred via the nodal points; the displacements of the nodes are the unknowns in the problem [28].

HCF: High Cycle Fatigue; fatigue occurring as a result of loads applied in the elastic range with fatigue lives greater than 10,000 cycles [1:1].

Intrinsic Magnetic Field: the magnetic field of a magnet at one of its poles; when a gaussmeter is used to measure the intrinsic magnetic field of a magnet, the gaussmeter's probe should be touching one of the poles.

LCF: Low Cycle Fatigue; fatigue occurring as a result of the application of high loads (nonelastic range) with fatigue lives less than 10,000 cycles [1:1].

Magnetic Dipole: every magnet, regardless of its shape, has two poles: north and south, which exhibit forces on each other (like poles repel, opposite poles attract) [14:805]; while every magnet is a dipole, since the magnetic field lines run through the magnet as well as enter and exit it, at close distances the magnet will not exhibit "true dipole" behavior; however, at larger distances (typically, five times, or greater, the largest dimension of the magnet [22]), the magnet can be modeled as a magnetic dipole.

Magnetic Dipole Moment (or magnetic moment): a mathematical representation of a magnet used to predict the magnetic field at a distance from its source; generally the distance to the measurement point is much greater than the largest dimension of the magnet; the error of this technique is roughly less than 2% for distances greater than five times the largest dimension of the magnet [22].

Magnetic Field (or magnetic flux density): the magnetic flux per unit area; tiny current loops created by electrons rotating about a nucleus effectively set up magnetic fields through their rotational axis; a magnetic field vector at some point in space can be

defined in terms of a magnetic force that would be exerted on an appropriate test object; for example, a 1 coulomb charge moving through a field of 1 tesla with a velocity of 1 m/s perpendicular to the field experiences a force of 1 newton [14:806-808, 852].

Magnetic Flux: the amount of magnetic field lines entering or exiting a closed surface; magnetic field lines due to current loops do not begin or end at any point, as such no isolated magnetic pole has ever been detected, and perhaps does not even exist; therefore, the net magnetic flux through any closed surface is always zero (the number of lines entering the closed surface is equal to the number of lines exiting the surface) [14:849, 852-854].

Magnetic Permeability: a constant representing a substance's susceptibility to magnetization [14:855, 856]; materials with high magnetic permeabilities (iron, nickel, cobalt) are used to make permanent magnets.

Magnetization Vector: a quantity which describes the magnetic state of a substance; the magnitude of the magnetization vector is equal to the magnetic moment per unit volume of the substance

Permeability of Free Space: a constant representing the effect free space (a vacuum) has on the magnetic field lines of a magnet [14:836]; essentially, free space allows the field lines to flow unaltered.

RMS: Root Mean Square; the square root of the average value of a squared quantity; if the quantity A is measured, $A_{rms} = \sqrt{\overline{A^2}}$ [14:564].

TEFF: Turbine Engine Fatigue Facility, Air Force Research Laboratory, Wright-Patterson Air Force Base, OH

Appendix B: Incorrect Dimensional (Units) Derivation of Axial Magnetic Field

When using, or deriving, any equation, it is important to make sure the units match. Starting with Equation 3 (see Chapter II for derivation), it can be broken down into an equation of units as follows (see lists of units and symbols for explanation of symbols and their associated units):

$$B = \frac{m_o \cdot I \cdot n}{2(R_2 - R_1)}\left[x_2 \ln \frac{\sqrt{R_2^2 + x_2^2} + R_2}{\sqrt{R_1^2 + x_2^2} + R_1} - x_1 \ln \frac{\sqrt{R_2^2 + x_1^2} + R_2}{\sqrt{R_1^2 + x_1^2} + R_1} \right] \tag{3}$$

$$T = \frac{(T \cdot m/A) \cdot A \cdot (turns/m)}{(m - m)}\left[m \cdot \ln \frac{\sqrt{m^2 + m^2} + m}{\sqrt{m^2 + m^2} + m} - m \cdot \ln \frac{\sqrt{m^2 + m^2} + m}{\sqrt{m^2 + m^2} + m} \right]$$

$$T = \frac{T}{m}\left[m \cdot \ln \frac{m}{m} - m \cdot \ln \frac{m}{m} \right]$$

$$T = \frac{T}{m} \cdot m = T$$

With Equation 3 derived correctly, the units cancel on the right side of the equation, leaving teslas, the unit of measurement for the magnetic field on the left side of the equation. However, when the derivation is accomplished incorrectly, as shown on the following pages, the units will not cancel properly, indicating the derivation is incorrect.

The derivation begins once again with the Biot-Savart law:

$$d\vec{B} = k_m \frac{I \cdot d\vec{s} \times \hat{r}}{r^2} \tag{1}$$

It follows the same mathematical steps to derive the magnetic field of a circular loop, Equation 9:

$$B_x = \frac{m_o \cdot I \cdot R^2}{2 \cdot \left(x^2 + R^2\right)^{3/2}} \tag{9}$$

However, if the formula from this point on is derived strictly geometrically, as follows, the resultant equation ends up with incorrect units.

$$B = \oint dB_x = \frac{m_o \cdot N \cdot I}{2l} \int_{R_1}^{R_2} \int_{x_1}^{x_2} \frac{R^2}{\left(x^2 + R^2\right)^{3/2}} dx \cdot dR$$

integrating with respect to x yields [14:A.25]:

$$B = \frac{m_o \cdot N \cdot I}{2l} \int_{R_1}^{R_2} R^2 \cdot \left[\frac{1}{R^2} \cdot \left(\frac{x_2}{\sqrt{x_2^2 + R^2}} - \frac{x_1}{\sqrt{x_1^2 + R^2}} \right) \right] dR$$

integrating with respect to R yields [14:A.25]:

$$B = \frac{m_o \cdot N \cdot I}{2l} \cdot \left[x_2 \ln \frac{\sqrt{R_2^2 + x_2^2} + R_2}{\sqrt{R_1^2 + x_2^2} + R_1} - x_1 \ln \frac{\sqrt{R_2^2 + x_1^2} + R_2}{\sqrt{R_1^2 + x_1^2} + R_1} \right]$$

Accomplishing an analysis of units like that done with Equation 3 produces the following:

$$T = \frac{(T \cdot m/A) \cdot turns \cdot A}{m}\left[m \cdot \ln \frac{\sqrt{m^2 + m^2} + m}{\sqrt{m^2 + m^2} + m} - m \cdot \ln \frac{\sqrt{m^2 + m^2} + m}{\sqrt{m^2 + m^2} + m} \right]$$

$$T = T\left[m \cdot \ln \frac{m}{m} - m \cdot \ln \frac{m}{m} \right]$$

$$T = T \cdot m$$

From this analysis of units, it is seen the units on the right side of the equation, when derived incorrectly, do not equal the units on the left side of the equation. This provides a good indication the derivation was accomplished incorrectly and needs to be accomplished correctly as shown in Chapter II.

Appendix C: Sample Mathcad™ Spreadsheet for Magnetic Field and Torque Calculations with Varying Current

$\mu_o := 4 \cdot \pi \cdot 10^{-7}$ Wb/A-m $\quad r_1 := .875 \cdot .0254 \quad r_1 = 0.022225$ m

$I := 2..20$ A $\quad r_2 := 2 \cdot .0254 \quad r_2 = 0.0508$ m

$turnsperinch := \frac{408}{1.96} \quad turnsperinch = 208.163$

$turnspermeter := turnsperinch \div .0254 \quad turnspermeter = 8195 \quad n := 8195$ turns/m

$B_{top} := .318$ T $\quad B_{bottom} := .322$ T

$B_i := (B_{top} + B_{bottom}) \div 2 \quad B_i = 0.32$ T

$x_1 := (.125 + 5 \div 32) \cdot .0254 \quad x_1 = 0.00714375$ m

$x_2 := (2.125 + 5 \div 32) \cdot .0254 \quad x_2 = 0.05794375$ m

$r := .125 \cdot .0254 \quad r = 3.175 \times 10^{-3}$ m $\quad l := (2 \cdot .125 + .05) \cdot .0254 \quad l = 7.62 \times 10^{-3}$ m

$V := \pi \cdot r^2 \cdot l \quad V = 2.413194 \times 10^{-7}$ m^3 $\quad m := \frac{B_i \cdot V}{\mu_o} \quad m = 0.061451$ $A \cdot m^2$

$$B_{air_I} := \frac{\mu_o \cdot I \cdot n}{2 \cdot (r_2 - r_1)} \cdot \left(x_2 \cdot \ln\left(\frac{\sqrt{r_2^2 + x_2^2} + r_2}{\sqrt{r_1^2 + x_2^2} + r_1} \right) - x_1 \ln\left(\frac{\sqrt{r_2^2 + x_1^2} + r_2}{\sqrt{r_1^2 + x_1^2} + r_1} \right) \right)$$

$k_{iron} := 1.787304$

$$B_{iron_I} := \frac{k_{iron} \cdot \mu_o \cdot I \cdot n}{2 \cdot (r_2 - r_1)} \cdot \left(x_2 \cdot \ln\left(\frac{\sqrt{r_2^2 + x_2^2} + r_2}{\sqrt{r_1^2 + x_2^2} + r_1} \right) - x_1 \ln\left(\frac{\sqrt{r_2^2 + x_1^2} + r_2}{\sqrt{r_1^2 + x_1^2} + r_1} \right) \right)$$

$k_{steel} := 1.790887$

$$B_{steel_I} := \frac{k_{steel} \cdot \mu_o \cdot I \cdot n}{2 \cdot (r_2 - r_1)} \cdot \left(x_2 \cdot \ln\left(\frac{\sqrt{r_2^2 + x_2^2} + r_2}{\sqrt{r_1^2 + x_2^2} + r_1} \right) - x_1 \ln\left(\frac{\sqrt{r_2^2 + x_1^2} + r_2}{\sqrt{r_1^2 + x_1^2} + r_1} \right) \right)$$

Appendix D: Sample Mathcad™ Spreadsheet for Magnetic Field and Torque Calculations for Increasing Gap between Coil and Permanent Magnets

$\mu_o := 4 \cdot \pi \cdot 10^{-7}$ Wb/A-m $r_1 := .875 \cdot .0254$ $r_1 = 0.022225$ m $n := 8195$ turns/m

$I := 5$ A $d := 0..50$ $r_2 := 2 \cdot .0254$ $r_2 = 0.0508$ m $Bi := .32$ T

$xl_d := (.125 + d \div 10) \cdot .0254$ $x2_d := (2.125 + d \div 10) \cdot .0254$ $r := .125 \cdot .0254$

$r = 3.175 \times 10^{-3}$ m

$$B_d := \frac{\mu_o \cdot I \cdot n}{2 \cdot (r_2 - r_1)} \cdot \left[x2_d \cdot \ln\left[\frac{\sqrt{r_2^2 + (x2_d)^2} + r_2}{\sqrt{r_1^2 + (x2_d)^2} + r_1} \right] - xl_d \cdot \ln\left[\frac{\sqrt{r_2^2 + (xl_d)^2} + r_2}{\sqrt{r_1^2 + (xl_d)^2} + r_1} \right] \right]$$

$l := (2 \cdot .125 + .05) \cdot .0254$ $V := \pi \cdot r^2 \cdot l$ $m := \frac{Bi \cdot V}{\mu_o}$

$l = 7.62 \times 10^{-3}$ m $V = 2.413194 \times 10^{-7}$ m^3 $m = 0.061451$ $A \cdot m^2$ $\tau_d := m \cdot B_d$

$k_{iron} := 1.787304$ $k_{steel} := 1.790887$

$Biron_d := k_{iron} \cdot B_d$ $Bsteel_d := k_{steel} \cdot B_d$

Appendix E: Dimensions of Aluminum Spindle and Ferromagnetic Core

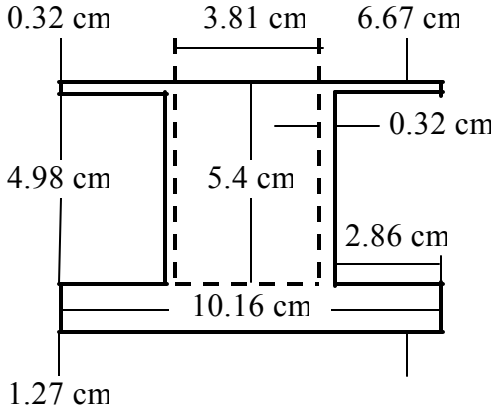

Spindle
Side View

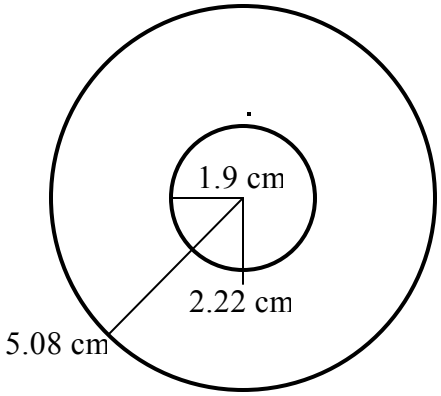

Spindle
Top View

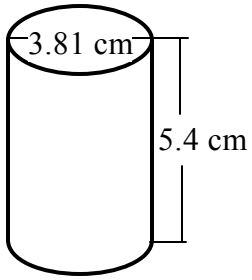

Ferromagnetic
Core

With the design given by the TEFF, the wire is wrapped on the aluminum spindle which has a hollow center. The ferromagnetic cores are then inserted in the hollow core of the aluminum spindle.

Bibliography

1. Ivancic, Frank T. *The Effect of a Hard Coating on the Damping and Fatigue Life of Titanium*. MS thesis, AFIT/GAE/ENY/03-12. Graduate School of Engineering and Management, Air Force Institute of Technology (AU), Wright-Patterson AFB OH, March 2003 (AD-A412854).

2. Grady, Joseph E. "Fundamentals of High-Cycle Fatigue," *Machine Design*, 71:86 (1999).

3. Ritchie, R. O., B. L. Boyce, J. P. Campbell, O. Roder, A. W. Thompson, and W. W. Mulligan. "Thresholds for High Cycle Fatigue in a Turbine Engine Ti-6Al-4V Alloy," *International Journal of Fatigue*, 21:653-662 (1999).

4. Nicholas, T. and J. R. Zuiker. "On the Use of the Goodman Diagram for High Cycle Fatigue Design," *International Journal of Fracture*, 80:219-235 (1996).

5. Shen, M. H. Herman. "Development of a Free Layer Damper Using Hard Coatings," *Proceedings, 7th National Turbine Engine High Cycle Fatigue Conference*, May 2002.

6. Zabierek, Donald. "Damping Test Capabilities at the Turbine Engine Fatigue Facility (TEFF)." 2003.

7. Jones, Keith, Charles Cross, Tommy George, and Brian Runyon. "Automated Identification of the Temperature, Frequency, and Strain Dependencies of Damping Treatments." May 2003.

8. Torvik, P. J., S. Patsias, and G. R. Tomlinson. "The Evaluation of Damping of Coated Beams: Comparison of Two Methodologies," *Proceedings, 7th National Turbine Engine High Cycle Fatigue Conference*, May 2002.

9. ASTM Standard: E 756, Standard Test Method for Measuring Vibration-Damping Properties of Materials, ASTM International, Conshohocken PA, 10 September, 1998.

10. Palazotto, Anthony. Professor of Aeronautics and Astronautics, Air Force Institute of Technology, Wright-Patterson Air Force Base, OH. Personal Corresondence, 2003.

11. Chew, Meng-Seng, Li-Farn Yang, and Jer-Nan Juang. "Suspension Devices for Vibration Testing of Structures." www.nasatech.com/Briefs/July99/LAR14272.

12. Groves, Clark W. Assistant Professor of Physics, Air Force Institute of Technology, Wright-Patterson Air Force Base OH. Personal Correspondence, October 2003.

13. Wood, William D. Assistant Professor of Electrical Engineering, Air Force Institute of Technology, Wright Patterson Air Force Base OH. Personal Correspondence, 3 Dec 2003.

14. Serway, Raymond A. *Physics For Scientists & Engineers* (3rd Edition). Philadelphia: Saunders College Publishing, 1990.

15. Kurtus, Ron. "Creating Electromagnetism." www.school-for-champions.com/science/electromagnetism, 9 August 2002.

16. www.whatis?com.com/permeability. whatis.com *Target Search*^{TM}, Tech Target Network, 20 April 2001.

17. "Permanent Magnet & Electromagnet Principles." www.rondout.k12.ny.us/cmooers/Electronics/magnetism.ppt. Electricity/Electronics Technology Department, Rondout Valley High School, Accord NY.

18. "Magnetic Properties of Solids." http://hyperphysics.phy-astr.gsu.edu/hbase/solids/magpr.html.

19. "Long Range Order in Ferromagnets." http://hyperphysics.phy-astr.gsu.edu/hbase/solids/ferro.html.

20. "Iron Core Solenoid." http://hyperphysics.phy-astr.gsu.edu/hbase/magnetic/elemag.html.

21. Dennison, Eric. "Axial Field of a Finite Solenoid." www.netdenizen.com/emagnet/solenoids/solenoidaxis.htm.

22. "Off-Axis Field Due to a Magnetic Dipole Moment." www.netdenizen.com/emagnet/offaxis/mmoffaxis.htm.

23. Dennison, Eric. Principal Engineer, Software Design, Tyco Safety Products, Tyco International. Electronic Message, 3 December 2003.

24. Dennison, Eric. "Axial Field of a Finite, Straight, Thin Shell Solenoid." www.netdenizen.com/emagnet/solenoids/thinsolenoid.htm.

25. Groom, Nelson J. "Expanded Equations for Torque and Force on a Cylindrical Permanent Magnet Core in a Large-Gap Magnetic Suspension System." NASA Technical Paper 3638, February 1997.

26. "Experiments with Electromagnets." www.my.execpc.com/~rhoadley/magelect.htm

27. *The American Heritage Dictionary* (2nd College Edition). Boston: Houghton Mifflin Company, 1985.

28. Broek, David. *Elementary Engineering Fracture Mechanics* (4th Revised Edition). Hingham MA: Kluwer Academic Publishers, 1986.

29. *MG-4d Portable Hand-held Gaussmeter Instruction Manual*. Worcester MA: Walker LDJ Scientific, Inc, no date.

30. Jones, Keith. Professor, United States Air Force Academy, Colorado Springs CO. Personal Correspondence. March 2003.

Vita

Capt Todd M. Hoover graduated from Williamsport Area High School in Williamsport, PA. He entered undergraduate studies at the United States Air Force Academy in Colorado Springs, CO where he graduated with a Bachelor of Science degree in Basic Sciences and was commissioned in June 1994.

His first assignment was at F.E. Warren AFB, WY with the 320th Missile Squadron as a Missile Launch Officer in November 1994. In May 1999, he was assigned to the 4th Space Operations Squadron, Schriever AFB, CO as a Milstar Satellite Vehicle Operator. In August 2002, he entered the Graduate School of Engineering and Management, Air Force Institute of Technology. Upon graduation, he will be assigned to the Space and Missile Systems Center at Los Angeles AFB, CA.

REPORT DOCUMENTATION PAGE

Form Approved
OMB No. 074-0188

The public reporting burden for this collection of information is estimated to average 1 hour per response, including the time for reviewing instructions, searching existing data sources, gathering and maintaining the data needed, and completing and reviewing the collection of information. Send comments regarding this burden estimate or any other aspect of the collection of information, including suggestions for reducing this burden to Department of Defense, Washington Headquarters Services, Directorate for Information Operations and Reports (0704-0188), 1215 Jefferson Davis Highway, Suite 1204, Arlington, VA 22202-4302. Respondents should be aware that notwithstanding any other provision of law, no person shall be subject to an penalty for failing to comply with a collection of information if it does not display a currently valid OMB control number.
PLEASE DO NOT RETURN YOUR FORM TO THE ABOVE ADDRESS.

1. REPORT DATE *(DD-MM-YYYY)*	**2. REPORT TYPE**	**3. DATES COVERED** *(From – To)*
23 Mar 2004	Master's Thesis	30 Aug 2002 – 23 Mar 2004

4. TITLE AND SUBTITLE

AN ELECTROMAGNETIC TOOL FOR DAMPING AND FATIGUE ANALYSIS

5a. CONTRACT NUMBER

5b. GRANT NUMBER

5c. PROGRAM ELEMENT NUMBER

6. AUTHOR(S)

Hoover, Todd M., Captain, USAF

5d. PROJECT NUMBER

5e. TASK NUMBER

5f. WORK UNIT NUMBER

7. PERFORMING ORGANIZATION NAMES(S) AND ADDRESS(S)
Air Force Institute of Technology
Graduate School of Engineering and Management (AFIT/EN)
2950 Hobson Way
WPAFB OH 45433-7765

8. PERFORMING ORGANIZATION REPORT NUMBER

AFIT/GSS/ENY/04-M04

9. SPONSORING/MONITORING AGENCY NAME(S) AND ADDRESS(ES)
Air Force Research Laboratory/PRPG
Attn: Dr. Charles Cross
1950 Fifth Street AFRL-PRPG
WPAFB OH 45433 DSN: 785-6241

10. SPONSOR/MONITOR'S ACRONYM(S)

11. SPONSOR/MONITOR'S REPORT NUMBER(S)

12. DISTRIBUTION/AVAILABILITY STATEMENT
APPROVED FOR PUBLIC RELEASE; DISTRIBUTION UNLIMITED.

13. SUPPLEMENTARY NOTES

14. ABSTRACT

An automated test system was developed by the USAF Turbine Engine Fatigue Facility (TEFF). This system was initially designed to reduce the time and manpower required to characterize damping treatments. It is based on a digitally controlled environmental chamber with automated data acquisition and processing. Several outputs are available including identification of natural frequencies, modal damping ratios from the acquired frequency responses, and changes in damping with response amplitude; however, the TEFF additionally desires the capability to study fatigue under a free boundary condition.

The system consists of a test specimen suspended by a pendulum to closely simulate free boundary conditions and to minimize the dissipation of vibrational energy. Two rare earth magnets are attached to a specimen. The magnetized end is inserted into an orthogonal magnetic field produced by an electromagnet. Alternating the current oscillates the direction of the magnetic field by 180 degrees. The effect of the electromagnet's magnetic field on the specimen's magnets is the application of a torque; as this torque alternates directions, it excites vibration in the beam. This torque, while useful, was not fully understood. The purpose of this thesis is threefold: 1. Develop an equation to predict the magnetic field produced by an electromagnetic coil; 2. Develop an equation for predicting the torque exerted on the beam; and 3. Experimentally validate the accuracy of these equations.

15. SUBJECT TERMS
Free-free Boundary Conditions; Fatigue; High Cycle Fatigue; Damping; Viscoelastic Constrained Layer Damping; Vibration; Magnetic; Electromagnetic; Solenoid; Ferromagnetic

16. SECURITY CLASSIFICATION OF:			**17. LIMITATION OF ABSTRACT**	**18. NUMBER OF PAGES**	**19a. NAME OF RESPONSIBLE PERSON**
REPORT	**ABSTRACT**	**c. THIS PAGE**			Anthony Palazotto
U	**U**	**U**	**UU**	109	**19b. TELEPHONE NUMBER** *(Include area code)* (937) 255-3636, ext 4599; e-mail: Anthony.Palazotto@afit.edu

Standard Form 298 (Rev: 8-98)
Prescribed by ANSI Std. Z39-18